

AN ABSTRACT OF THE THESIS OF

Sean Casey for the degree of Master of Science in Mechanical Engineering
presented on June 6, 2013.

Title: Modeling, Simulation, and Analysis of Two Hydraulic Power Take-off
Systems for Wave Energy Conversion

Abstract approved: _____
Robert K. Paasch

Hydraulic power take-off (PTO) systems have been implemented in several wave energy converter (WEC) designs in recent years. Two popular hydraulic PTO configurations coupled to a point absorber hydrodynamic model are simulated in waves representative of an energetic sea state likely to be found in deep waters off the coast of Oregon. The first hydraulic PTO configuration is a passive system tuned to the dominant forcing period of the sea state. The second system is an actively controlled hydraulic PTO topology tracking an optimal power absorption trajectory. A linear quadratic tracking controller is developed to follow the reference trajectory and performs well despite the nonlinear elements of the system dynamics. Simulation results of the system dynamics are presented for both models. A loading analysis is conducted and loading distributions of the two systems in irregular waves are compared. The distributions show the active system to have a larger variability in loading, while the distributions of the passive system indicate more frequent mean loading components. Parameters of the passive system components are varied in order to understand the effect on power output and loading.

©Copyright by Sean Casey
June 6, 2013
All Rights Reserved

Modeling, Simulation, and Analysis of Two Hydraulic Power
Take-off Systems for Wave Energy Conversion

by

Sean Casey

A THESIS

submitted to

Oregon State University

in partial fulfillment of
the requirements for the
degree of

Master of Science

Presented June 6, 2013
Commencement June 2014

Master of Science thesis of Sean Casey presented on June 6, 2013.

APPROVED:

Major Professor, representing Mechanical Engineering

Head of the School of Mechanical, Industrial, & Manufacturing Engineering

Dean of the Graduate School

I understand that my thesis will become part of the permanent collection of Oregon State University libraries. My signature below authorizes release of my thesis to any reader upon request.

Sean Casey, Author

ACKNOWLEDGEMENTS

I am forever indebted to those who have provided friendship, love, and knowledge throughout my life and supported me throughout my educational pursuits. I have an enormous debt of gratitude to my family, for never ceasing to be there with love and kindness even when times were tough. My parents instilled in me a passion for the pursuit of knowledge and have continually supported my creative endeavours. The abundance of books in our home growing up, especially those on physics and philosophy, sparked my scientific interests and love of knowledge. To my brother and sisters, thank you for being stand-up role models whose successes have motivated me to achieve my own goals.

I thank the many friends I've had over the years for giving me a chance to grow, discover, and create with them. From weekend adventures camping and skiing to multi-week climbing trips, we have truly had some excellent times. The friendship and kindness has made Oregon a wonderful place to live and work.

I would like to thank my colleagues at the Northwest National Marine Renewable Energy Center, especially Blake Boren and Adam Brown—our conversations on marine energy have helped direct some of this research. Thank you to Blake Boren and Erin Collins for reading through this thesis and providing corrections and suggestions for improvement.

A sincere thanks to all the teachers I've had the privilege of studying under, especially my advisors Dr. Belinda Batten and Dr. Robert Paasch for providing an excellent graduate experience and funding. Thank you to Dr. Ross Hatton and Dr. Ted Brekken for sitting on my committee and providing direction along the way. And finally, I am sincerely thankful to all the researchers and pursuers of knowledge who have come before me:

"If I have seen further it is by standing on the shoulders of giants."

—Isaac Newton

Disclaimer: This material is based upon work supported by the Department of Energy under Award Number DE-FG36-08GO18179. This report was prepared as an account of work sponsored by an agency of the United States Government. Neither the United States Government nor any agency thereof, nor any of their employees, makes any warranty, expressed or implied, or assumes any legal liability or responsibility for the accuracy, completeness, or usefulness of any information, apparatus, product, or process disclosed, or represents that its use would not infringe privately owned rights. Reference herein to any specific commercial product, process, or service by trade name, trademark, manufacturer, or otherwise does not necessarily constitute or imply its endorsement, recommendation, or favoring by the United States Government or any agency thereof. Their views and opinions of the authors expressed herein do not necessarily state or reflect those of the United States Government or any agency thereof.

TABLE OF CONTENTS

	<u>Page</u>
1 Introduction	1
1.1 Wave Energy Conversion	1
1.2 A Review of Modeling and Simulation of WECs	3
1.2.1 Ocean Wave Mechanics	4
1.2.2 Wave Forces on Floating Structures	5
1.2.3 Power Take Off Systems	7
1.2.4 Control of Wave Energy Converters	10
1.3 Contribution of this Thesis	11
2 System Modeling	13
2.1 Introduction	13
2.2 Wave Modeling	14
2.2.1 Regular Waves	15
2.2.2 Irregular Waves	15
2.3 Hydrodynamic Modeling of a Cylindrical Buoy	17
2.4 Hydraulic Power Transmission Modeling	18
2.4.1 Passive Hydraulic PTO	19
2.4.2 Active Hydraulic PTO	22
3 Simulation Results	27
3.1 Time Domain Simulation	27
3.2 System Parameters	27
3.3 System Response	30
4 System Analysis	33
4.1 Loading Analysis of the Nominal Systems	33
4.2 Variation of System Parameters for the Passive System	41
4.2.1 Variation of Generator Damping	42
4.2.2 Variation of Motor Displacement	44
4.2.3 Variation of High Pressure Accumulator Volume	46
4.2.4 Variation of Pump Area	48
5 Conclusions and Future Work	50

TABLE OF CONTENTS (Continued)

	<u>Page</u>
Bibliography	53
Appendices	57
A Design Equations for the WEC Systems	58

LIST OF FIGURES

<u>Figure</u>	<u>Page</u>
1.1 An example of a heaving body point absorber system. An incident wave causes the buoy to heave upwards creating relative motion between the damping plate and the buoy. The PTO then converts this mechanical kinetic energy into electrical energy.	2
1.2 High level functional block diagram of a WEC system. The PTO system is assumed to provide the mooring, therefore it is not explicitly shown.	4
2.1 A high level system schematic. The hydraulic PTO is assumed fixed while the floating body can move in the heave direction.	13
2.2 Schematic of a monochromatic wave.	14
2.3 Modified Bretschneider-Mitsuyasu spectrum with $H_s = 3\text{m}$ and $T_s = 10\text{s}$ used to model irregular waves.	16
2.4 Schematic of the passive WEC system. The arrows indicate the direction of flow.	19
2.5 Valve opening behaviour as a function of pressure difference across the valve.	21
2.6 Schematic of the active WEC system.	22
3.1 System kinematics and optimum velocity trajectory in regular and irregular waves.	31
3.2 Excitation and piston forcing in regular and irregular waves.	31
3.3 Power output for the passive and active hydraulic PTO systems.	32
3.4 System pressure and forcing when the stalling effect occurs in the passive system. A check valve is open when either pressure in sides A or B are greater than side C or less than side D.	32
4.1 An example of a purely sinusoidal fully reversed stress time series. The amplitude, σ_a , and the mean value, σ_m , characterize the stress history.	34

LIST OF FIGURES (Continued)

<u>Figure</u>	<u>Page</u>
4.2 An example S-N curve for 316 stainless steel. The knee of the curve is called the endurance limit. Any calculated fatigue strength cycles below this point will not contribute to fatigue damage. The sloped region of the curve constitutes the finite-life regime where cycles will contribute to damage.	34
4.3 Time series of the loading for the two systems in irregular waves with a significant height of 3 meters and an energy period of 10 seconds.	36
4.4 Piston and generator mean and amplitude loading distributions for a 30 minute irregular sea state.	37
4.5 Loading distribution of the passive system with respect to mean and amplitude values for irregular waves with a significant height of 3 meters and an energy period of 10 seconds.	39
4.6 Loading distribution of the active system with respect to mean and amplitude values for irregular waves with a significant height of 3 meters and an energy period of 10 seconds.	40
4.7 The exceedance probability of the rainflow counted loading cycles for irregular waves with a significant height of 3 meters and an energy period of 10 seconds.	41
4.8 Loading distribution as the generator damping is changed. All other parameters are the same as listed in Tables 3.1 through 3.3.	43
4.9 Average power and loading values as the generator damping is varied.	43
4.10 Loading distribution as the motor displacement ratio is changed. At $\alpha = 1$ the motor displacement is $250cm^3$. All other parameters are the same as listed in Tables 3.1 through 3.3.	45
4.11 Average power and loading values as the motor displacement ratio is varied.	45
4.12 Loading distribution as the high pressure accumulator volume is changed. At $v_{C0} = 7.5m^3$ the original system is shown. All other parameters are the same as listed in Tables 3.1 through 3.3.	47

LIST OF FIGURES (Continued)

<u>Figure</u>	<u>Page</u>
4.13 Average power and loading values as the high pressure accumulator volume is varied.	47
4.14 Loading distribution as the pressurized pump area fraction is changed. The pump area fraction is with respect to the original pump size. At $A_p = 1$ the original system is shown. All other parameters are the same as listed in Tables 3.1 through 3.3.	49
4.15 Average power and loading values as the generator pump area fraction is varied.	49

LIST OF TABLES

<u>Table</u>	<u>Page</u>
3.1 Simulation parameters used for the point absorber buoy model. . .	28
3.2 Simulation parameters used for the passive hydraulic PTO system. .	29
3.3 Simulation parameters used for the active hydraulic PTO system. .	29
3.4 Average power input and output of each system.	30
4.1 Piston and generator loading statistics for each system.	38

Chapter 1: Introduction

1.1 Wave Energy Conversion

The ocean is a vast, largely untapped energy resource where the conversion of clean renewable energy from ocean waves is possible. The immense power of ocean waves originates from the sun. Winds from the uneven solar heating of the earth create ripples on the ocean surface. These ripples build over time eventually creating the larger swells typically seen making their way to shore. At each energy conversion step, from sun to wind to wave, the energy density increases. Ocean waves dissipate very little energy as they traverse the seas, allowing fairly accurate forecasting models several days ahead. The high energy density combined with the ability for accurate predictions make ocean waves an attractive resource to complement the world's energy portfolio. A recent assessment estimates the global wave power resource to be approximately 3 TW [20], which represents an appreciable portion of the present global electrical power demand of approximately 15 TW [14]. In recent years, a large research push has been initiated world-wide to facilitate the commercialization of ocean wave energy.

Wave energy converters (WECs) are technologies aimed at harnessing the power from ocean waves. Thousands of WEC technologies have been patented [18], though few have ever been tested in real ocean waves at full scale. The technologies are largely in the research and development phase, and the industry has not converged on a common technological archetype. Wave energy converters can however be broadly classified into three main types: oscillating bodies, oscillating water columns, and over-topping devices [6]. For an overview of the various wave energy conversion technologies see [4, 6, 18].

This work will focus on a particular type of oscillating body called a heaving body point absorber, an example of which can be seen in Figure 1.1. The device

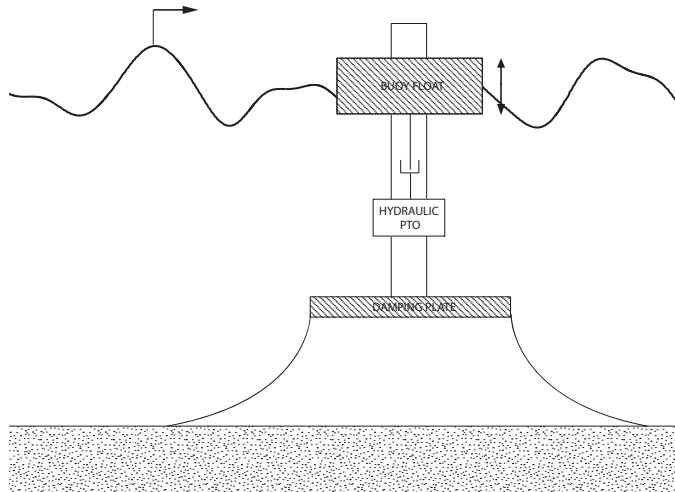


Figure 1.1: An example of a heaving body point absorber system. An incident wave causes the buoy to heave upwards creating relative motion between the damping plate and the buoy. The PTO then converts this mechanical kinetic energy into electrical energy.

uses resisted relative motion between the floating body and a reference point to absorb power. The reference point can be a large area mass in the case of two body point absorbers [33], or fixed to the ocean floor [17, 30]. In this work it is assumed the reference point is fixed to the ocean floor, or the large mass is perfectly damped and does not affect the response of the floating body. The floating body is assumed to operate in the heave direction to ease the hydrodynamic formulation and because it is the primary direction of power capture.

The resisting mechanism that converts the motion into electrical power is called the power take-off (PTO) system. Various PTO technologies have been implemented and studied from directly driven generators and mechanical transmissions [26, 27], pneumatic turbines [23], to hydraulic circuits connected to induction generators [9, 10, 30]. In this work, hydraulic PTO systems are modeled and simulated to gain insight into the loading and power characteristics of two popular configurations.

Capturing the power from ocean waves poses many difficult engineering chal-

lenges. The harsh and unforgiving ocean environment demands technologies that can withstand peak loadings many times greater than average. A WEC must be highly reliable, as any repairs at sea will be costly. Unplanned maintenance or repair in an ocean environment will most likely be an expensive undertaking [35]. Inclement weather may prohibit access to a device, and lost electricity production will compound costs. The repair or retrieval of a device at sea will only likely occur during opportune weather windows of low sea states [25], which could cause long periods of downtime and lost production if a device fails. In addition to high reliability and survivability, a device must also maintain high energy production over a range of sea-states. Several other key challenges including robust mooring design, life-cycle assessments, and the understanding of environmental effects must be addressed as well. For a thorough assessment of the challenges associated with the commercialization and implementation of WEC technologies and potential avenues to overcome these challenges see [21, 31]. An integral part to addressing these issues will be through modeling and simulation of various WEC systems to gain insight into the potential design requirements and issues before investing large sums of capital into physical prototypes.

1.2 A Review of Modeling and Simulation of WECs

A dynamic WEC model can be functionally decomposed into four main systems: ocean wave mechanics, floating body dynamics, power take off technology, and control systems. A functional decomposition can be seen in Figure 1.2. Ocean wave mechanics concerns the mathematical description of ocean waves and their evolution over time and space. Floating body dynamics involves the study of fluid structure interaction (FSI) where the fluid affects the device, and the fluid is simultaneously affected by the device. The topic of floating body dynamics is very complex, though simplifications can lead to fairly good engineering approximations. The PTO system is the internal machinery of the WEC which converts the mechanical motion of the floating body into electrical power. A WEC will most likely have some kind of control system in order to be efficient through a range of

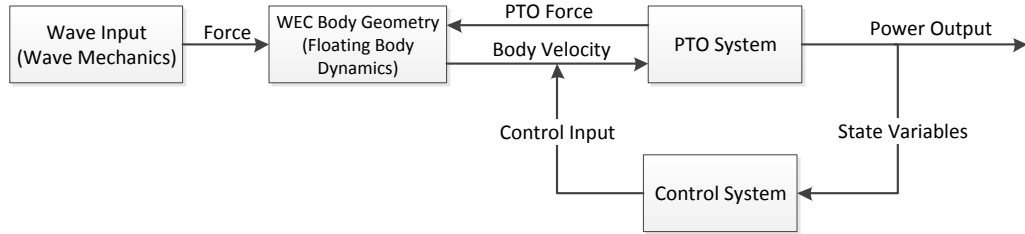


Figure 1.2: High level functional block diagram of a WEC system. The PTO system is assumed to provide the mooring, therefore it is not explicitly shown.

wave forcing frequencies. Another important WEC system is the mooring system, connecting the WEC to the ocean floor. In this study, the PTO system is assumed to provide the connection to the sea floor, and therefore the mooring system is not explicitly considered. An overview of the four functional systems follows with explanation of theory and the state of the art.

1.2.1 Ocean Wave Mechanics

To model a wave energy converter, one must first understand the nature of ocean waves. In the most complete treatment of the subject, the mechanics of water waves is most accurately described by the Navier-Stokes equations, however the equations typically have no closed form solution and computer simulations can be costly. Assuming the fluid to be incompressible, inviscid, and irrotational, allows for the development of a velocity potential [3]. The velocity potential can be employed in a boundary value problem to obtain a mathematical model of ocean waves. Further assuming the wave amplitude is much smaller relative to the wavelength, a valid assumption for ocean waves, a linear solution to the boundary value problem can be obtained. The solution of the boundary value problem leads to the dispersion relationship which relates the wavelength, or spatial frequency of the wave, to the wave period, or temporal frequency. In general waves of longer wavelength travel faster than those of shorter wavelength.

With the linearizing assumptions, ocean waves can be modeled as the superposition of many sinusoids traveling with different frequencies and direction. Measurements of the ocean surface elevation at a particular location in time will show a seemingly random wave pattern. However this pattern can be decomposed through a Fourier transform into a spectrum of energy components at different frequencies. Generalized spectra have been established which allow one to reconstruct a random wave field representative of actual ocean wave measurements.

Many authors have treated the subject of ocean wave modeling and mechanics. A fairly nontechnical overview can be found in [18], where the author presents the equations without derivation. The author also presents an overview of wave energy technology and derives theoretical power and efficiency values for canonical systems. A more technical study of wave mechanics can be found in [3], which provides a concise, thorough overview aimed for an audience of scientists and engineers. The author derives the equations for potential flow theory and wave mechanics from the governing laws by establishing the boundary value problem. Other texts such as [37] and [39] give in-depth analysis of random waves along with frequency spectrum reconstruction techniques and experimental methods.

The understanding of ocean wave mechanics allows one to develop the necessary input conditions for a WEC simulation model. The knowledge allows the engineer to develop devices that will meet the engineering requirements of the powerful and sometimes harsh ocean environment. Once the wave environment is developed, the interaction between the waves and a floating body must be understood.

1.2.2 Wave Forces on Floating Structures

The dynamics of a body floating in a fluid is an almost infinitely complex phenomenon, however simplifying assumptions lead to rather tractable solutions. Hydrodynamic and hydrostatic forces on the body occur from the presence of the changing pressure field of a wave and the movement of the body in the fluid. A body floating in the ocean is excited by a passing wave, and at the same time the body has some effect on the wave. If linear waves are assumed, the hydrodynamic

and hydrostatic forces can be decomposed into excitation, radiative damping, and buoyancy terms. The excitation force is a result of the incident wave and can be determined by integrating the hydrodynamic pressure field of the wave over the wetted area of the object at each instant in time while the device is held static. The radiation damping force is the result of the body oscillating in the fluid and producing waves that radiate away from the body. The radiation force can be determined by finding the force experienced by an oscillating body on a free surface in the absence of an excitation force. The buoyancy force is due to the hydrostatic pressure field as the device is displaced in a volume of water. Hydrodynamic coefficients relate the position, velocity, and acceleration of the body to the hydrodynamic and hydrostatic forces.

The derivation of the hydrodynamic coefficients is dependent on the floating body geometry. There are several simulation platforms which incorporate the floating body as a boundary condition in the solution of the velocity potential boundary value problem such as WAMIT, or ANSYS AQWA. Experimental techniques such as [15], used in this thesis, can also relate the hydrodynamic parameters of a particular body geometry to the incident wave properties. Finite element and computational fluid techniques have also been used to solve the fluid structure interaction problem, but are mainly reserved for high fidelity models where the device geometry and design are well established. These higher fidelity models require much more computational cost and the incorporation of control strategies will compound this cost. See [19] for a finite element technique applied to the modeling of a WEC.

Several authors have modeled various WEC prototypes using various techniques. The dynamics of oscillating heaving bodies was undertaken in depth by [7] where the author derives the equations of motion using complex analysis and a frequency domain approach. The author also derives the optimal power absorption conditions used in this thesis for a heaving point absorber WEC. One and two body heaving point absorbers were modeled in [32] where the floating body's impulse response functions were calculated using frequency domain software results.

The impulse response functions were then used to model the device in the time domain using ordinary differential equation (ODE) solvers. A simplified heaving point absorber was modeled in [1] in order to apply a model predictive control strategy. The author approximates the hydrodynamic coefficients as constants, an approach that will be used in this work as it allows straightforward implementation of control techniques. A thorough treatment of heaving body point absorber modeling can be found in [5] where the device was modeled in the time domain in conjunction with a hydraulic PTO system.

1.2.3 Power Take Off Systems

The mechanism to convert the mechanical motion of the floating body into electrical energy is called the power take-off (PTO) system. Power take-off systems for heaving body point absorbers can be broadly classified into three main categories: direct drive and mechanical, pneumatic, and hydraulic transmissions. Each type has benefits and drawbacks and in the end the choice will be driven by the functional requirements of the device, available resources, and economic costs.

1.2.3.1 Direct Drive and Mechanical Transmissions

Direct drive and mechanical PTO systems couple the force and speed of the buoy either directly to the generator or through a mechanical component such as a gearbox. The main attraction of direct drive and mechanical PTOs is the elimination of intermediate pneumatic or hydraulic conversion steps, thereby potentially increasing efficiencies and lowering system complexity. Direct drive and mechanical transmissions have been studied in [27] where 18 various designs were considered for a point absorber device and five were built and tested. Some of the designs studied were a windlass spindle, rack and pinion, and permanent magnet linear generators. The results of the analysis program indicated a permanent magnet linear generator to be a good choice for low power levels, however at higher power levels, air gap tolerances and material costs would be prohibitive. The study sug-

gested further exploration of a direct drive rotary machine which was then studied in [26].

1.2.3.2 Pneumatic Transmissions

Pneumatic PTO systems have been chiefly employed and studied in regards to oscillating water column (OWC) technologies [23]. The general concept involves using the oscillating pressure field of a wave to move air through a turbine. The wave may actuate a compliant surface, protecting the machinery from the corrosive salt water, or the free surface of the wave can be used directly. A Wells turbine is often employed because the rotational velocity is independent of airflow direction.

1.2.3.3 Hydraulic Transmissions

Hydraulic PTO systems, studied in this thesis, use a hydraulic circuit connected to a rotary generator to transform the float motion into electrical power. The motion of the floating body is transformed into a pressurized flow using a hydraulic pump. The flow can then be conditioned using hydraulic equipment such as valves and accumulators. The flow is transformed into rotary motion with a hydraulic motor/pump used to spin a generator. Hydraulic PTO systems offer an attractive design solution to transform the low speeds and high forces of ocean waves into high speed rotational motion required by most modern day electrical machines. Several current WEC designs employ various hydraulic PTO topologies in part due to the high power to weight ratio, inherent robustness, and the ability to customize off-the-shelf components to meet the needs of a particular design [10, 30, 33].

Two main categories of hydraulic transmissions for wave energy conversion exist. A nearly constant pressure system, referred to as the passive system in this work, delivers a nearly constant pressure fluid flow over the hydraulic motor by employing large accumulators. Another transmission referred to as the active system in this work is a variable pressure topology that directly connects the pump to the motor. The system uses variable hydraulic motor displacement to actively

control the pressure of the system thereby affecting the dynamics of the float directly.

Hydraulic power transmissions similar to the passive system studied in this work have been examined previously in [5, 7, 9] where a single acting piston pump drives fluid through a hydraulic motor/pump and generator. The results indicate a promising contribution can be made by incorporating a hydraulic PTO in a point absorber WEC using a set of rectifying valves and accumulators. Later, [28] extended their work by incorporating a double acting piston pump, thereby allowing fluid to flow on both the up and down strokes to the high pressure side. The work in [9] compared a passive hydraulic system versus one incorporating a control strategy to bring the WEC velocity into phase with the excitation force. The work of [28] showed how a latching control could be implemented in the double acting system by incorporating accumulators on the pump side that could augment the pressure on the pump, thereby providing a limited reactive control.

A PTO topology similar to the active system studied in this work was examined in [30] where the piston pump is directly connected to the motor. The hydraulic circuit uses continuous control of the motor displacement and generator damping to regulate the force on the buoy and the velocity of the generator. If the system pressure was exceeded in the case of large waves, the excess pressure could allow fluid to flow into another circuit containing an accumulator and motor, thereby extracting the excess energy.

A comparison of the two systems analyzed in this thesis was conducted in [2] where idealized versions of the two systems were modeled and controlled in simulation. The analysis included efficiency maps and changed the parameters of the pump and hydraulic motor to determine the power characteristics of the two systems. A digital displacement pump/motor was also examined and proved to increase the efficiency of two systems. The results indicate the choice of hydraulic motor/pump is critical to the commercialization of the two systems. The treatment of the two systems in this thesis extends the work by including the accumulator gas dynamics of the passive system, optimal controller design of the active system,

and a loading comparison of both systems.

A review of several different hydraulic PTO topologies was studied in [38] where the author indicates the strengths and weakness of each system with respect to control, power conditioning, and technology readiness. The author also experimentally tests one hydraulic transmission on a linear test bench giving an exemplary efficiency table for the hydraulic cylinder.

1.2.4 Control of Wave Energy Converters

Control strategies for wave energy converters can be broadly categorized as passive or active techniques. Passive control amounts to fixing the natural frequency of the WEC to that of the dominant wave frequency where the device is to be located. An active control system on the other hand, continually adjusts the natural frequency of the WEC in real time to match that of the incident waves, thereby increasing power absorption.

Maximum power absorption by a point absorber WEC is obtained when the frequency of the device is matched to the frequency of the wave excitation force. In other words the maximum power absorption occurs when the velocity of the body is in phase with the wave excitation force [7]. In an actual irregular sea composed of many different frequencies, the PTO system must be continually tuned to the incident wave excitation force. This necessitates a controller for the PTO system that can adjust the WEC properties to the incident ocean waves. In order to optimally control a WEC, future wave information is needed because of the non-causal hydrodynamics of a floating body [7].

Passive and active control techniques were studied in [8] for a point absorber WEC and it was found that active control allows for more power capture in irregular seas. The author explored different ways of fixing the device natural frequency for passive control. In that study, a point absorber WEC was tuned to the energy frequency, peak frequency, and a weighted average of peak frequencies of the wave elevation. The study found that tuning the device to the peak frequency of the wave energy spectrum allowed greatest power capture in all sea-states studied.

Active control techniques were then studied by the author and it was found that a sliding discrete Fourier transform to estimate the incident frequency performed best in high-energy sea-states. The wave frequency was also estimated using a time series analysis by recording successive zero crossing periods and estimating the next wave period. A pseudo-derivative feedback controller was also implemented and performed marginally poorer in all sea states, but required much less system information as only the PTO velocity was needed. In the end a balance must be made between required system information and controller complexity.

1.3 Contribution of this Thesis

The National Renewable Energy Laboratory's Marine Hydrokinetic Roadmap calls for 23 GW of installed marine energy capacity by 2030 [31]. To meet this target, many technological hurdles must first be overcome. The roadmap cites the need to develop better control strategies for WECs to improve power capture and increase the reliability and survivability of devices in extreme events. To this end, the simulations and analyses in this work were developed to aid in the understanding of device loading and power characteristics using high-level dynamic models.

The motivation for this research stems from two observations. First, the major design objectives for WECs are to maximize power conversion and maintain high reliability and survivability in extreme ocean conditions, as any repairs in a maritime environment will be costly [35]. The second observation is that by maximizing power absorption, a WEC is exposed to more energetic seas and higher loadings. If the reliability and survivability of WECs is related to the nature of the loading on components, the question then arises; what are the benefits and drawbacks of a passively tuned system compared to one that is actively controlled? Specifically, what are the differences in the nature of loading and power absorption between a passively and actively controlled system?

This thesis will cover the modeling and simulation of a heaving body point absorber WEC coupled to two different hydraulic power take-off systems. The first system, referred to as the passive system is tuned *a priori* to the dominant

wave environment and uses hydraulic elements to condition the power output. The second system, referred to as the active system, continuously changes the system response to match an optimal power absorption velocity profile.

The passive system, was originally proposed in [7] and further developed in [5] and [28]. The passive system uses hydraulic components such as valves and accumulators to rectify the power and smooth the flow over a hydraulic motor/generator drive. In this work the pump is modeled using the continuity equation for a compressible fluid, and the valves are modeled using a pressure dependent valve area equation.

The active system is similar to one studied in [30], however no energy overflow system was modeled and a simplified model of a generator is used. This work develops a linear quadratic tracking controller for the active system that adjusts the generator damping and motor displacement in order to rectify the rotational motion of the generator and track an optimal buoy velocity trajectory.

The system response of the two systems to regular and irregular waves is first shown and discussed. The system loading is then analyzed using a rainflow counting algorithm to develop loading cycle probability distributions. The distributions allow one to immediately see the differences in peak to average loading and the potential design requirements and issues. A variation of system parameters for the passive system is then conducted to illustrate how the loading and power characteristics change.

This thesis is divided into five chapters. In Chapter 2 the modeling of the wave environment, wave forces, and two hydraulic PTO topologies is described along with the controller design for the active system. Chapter 3 discusses the simulation of the two systems along with results for the system response. Chapter 4 discusses the loading analysis and shows results for the two systems. A variation of parameters is then performed on the passive system to show how the loading is affected by changes in the generator damping, motor displacement, accumulator volume, and pump size. The final chapter will conclude the thesis providing areas for future study and research.

Chapter 2: System Modeling

2.1 Introduction

A wave energy converter can be modeled in the time domain using linear wave theory and by defining the system's equations of motion. Time series wave data is first modeled and used in conjunction with a floating body geometry to determine the wave excitation force on the body. Once the excitation force is determined, the equations of motion defining the WEC system can be solved using standard ordinary differential equation solvers.

In this work, a cylindrical point absorber buoy was modeled in two dimensional regular and irregular waves for both the passive and active hydraulic PTO systems. A high level schematic of the WEC system is shown in Figure 2.1. The buoy is

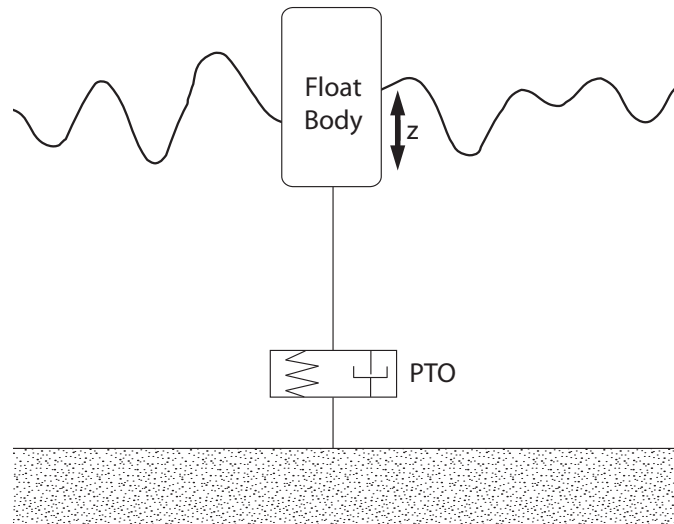


Figure 2.1: A high level system schematic. The hydraulic PTO is assumed fixed while the floating body can move in the heave direction.

excited in the heave direction by the incident waves, while the PTO is assumed fixed in place. The relative motion between the buoy and the PTO drives a hydraulic transmission, converting the linear heave energy into rotational energy harnessed by a generator.

This chapter will first explain the modeling of ocean waves and the determination of an excitation force for a cylindrical floating body. The modeling of two hydraulic PTO system topologies will then be developed. The design equations for the determination of the sizing of components and system parameters used in the simulations can be found in Appendix A.

2.2 Wave Modeling

Regular and irregular waves were modeled using linear wave theory, where it is assumed the wave heights are small compared to the wave length and the fluid is inviscid, irrotational, and incompressible [3]. Regular waves can be determined by simply specifying the wave height and period. Irregular waves on the other hand, are constructed from a wave frequency spectrum using the addition of several sinusoids chosen from the spectrum. A schematic of a regular wave including relevant wave parameters is shown in Figure 2.2. The wavelength, L , is the spatial

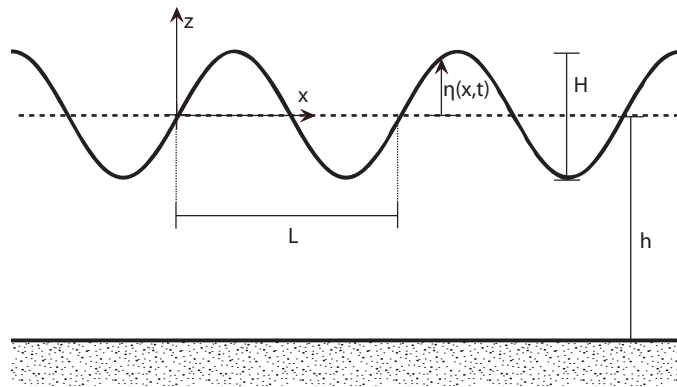


Figure 2.2: Schematic of a monochromatic wave.

length between two upward zero crossing points. The wave elevation at any point

in time along the x-axis is specified by η . The wave height, H , is the vertical distance between crest and trough. The depth, h , is a positive value specifying the distance from the sea-floor to the origin. The wave period, T , is temporal spacing between upward zero crossing points. These parameters will be used to develop time series wave profiles in the following sections.

2.2.1 Regular Waves

The surface displacement of a monochromatic, progressive wave as shown in the top plot of Figure 2.2, can be expressed as

$$\eta(x, t) = \frac{H}{2} \cos(kx - \sigma t) \quad (2.1)$$

$$k = \frac{2\pi}{L} \quad (2.2)$$

$$\sigma = \frac{2\pi}{T} \quad (2.3)$$

where H is the wave height, k is the spatial frequency, σ is the temporal frequency, and t is time. The spatial frequency is related to the wavelength, L , and the temporal frequency is related to the wave period, T . The spatial and temporal frequencies are related through the dispersion relationship expressed as,

$$\sigma^2 = gk \tanh(kh) \quad (2.4)$$

where g is the acceleration due to gravity, and h is the water depth. For this research deep water waves are assumed, therefore $\sigma^2 \approx gk$.

2.2.2 Irregular Waves

An irregular wave time series can be created by randomly phase shifting and superimposing several sinusoids of different heights and periods. The height and period of each constituent sinusoid can be derived from a frequency spectrum. Various

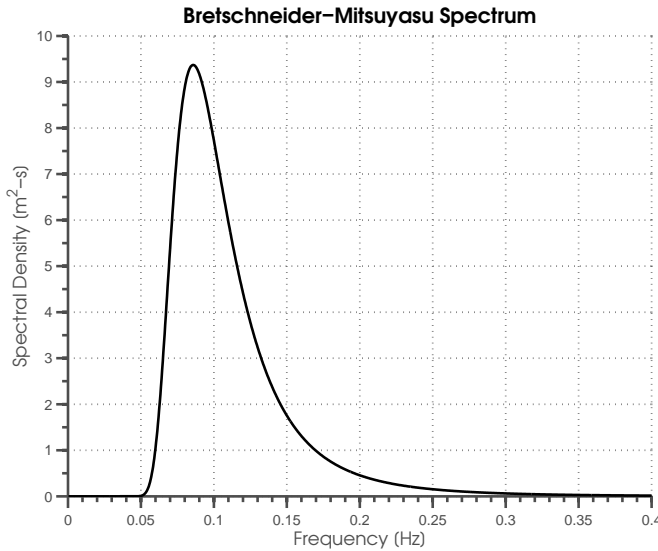


Figure 2.3: Modified Bretschneider-Mitsuyasu spectrum with $H_s = 3\text{m}$ and $T_s = 10\text{s}$ used to model irregular waves.

spectra have been created using empirical data to approximate different sea states. A modified Bretschneider-Mitsuyasu spectrum [39] was used in this work to model a sea state due to the ease and generality of its application. The spectrum is expressed as

$$s(f) = 0.257 \frac{H_s^2}{T_s^4 f^5} \exp\left(\frac{-0.75}{T_s f}\right) \quad (2.5)$$

where H_s is the significant wave height, T_s is the significant period, and f is the frequency of each component wave. The spectrum defines a fully-developed sea state where it is assumed the waves have reached a steady state condition where all transient forcing functions have died off. The spectrum used for the simulations can be seen in Figure 2.3.

Once the spectrum has been defined, the wave elevation of the i^{th} component wave can be found by

$$\eta_i = \sqrt{2s(f_i)\Delta f} \quad (2.6)$$

where Δf is the frequency spacing of the spectrum. To ensure the random wave

profile does not repeat, the frequency spacing is chosen to be $1/t_f$, where t_f is the desired simulation time. Using each component wave elevation and frequency, the overall irregular wave form can be described as

$$\eta = \sum_i \eta_i \cos(k_i x - \sigma_i t - \phi_i) \quad (2.7)$$

where ϕ_i is the random phase of the i^{th} wave component chosen from a uniform distribution on the interval $[0, 2\pi]$.

2.3 Hydrodynamic Modeling of a Cylindrical Buoy

A cylindrical floating body is modelled with a single degree of freedom in heave. Employing Newton's 2nd law, the buoy dynamics can be written as

$$m\ddot{z} = F_e + F_r + F_b + F_{pto} \quad (2.8)$$

where m is the dry mass of the buoy, \ddot{z} is the heave acceleration, F_e is the excitation force, F_r is the radiation damping, F_b is the buoyant force, and F_{pto} is the PTO force calculated from the hydraulic PTO models discussed in the next sections.

The excitation and radiation damping force, found using a linearized version of the Morison equations [1], can be written as

$$F_e = \mu\ddot{\eta} + \lambda\dot{\eta} + K\eta \quad (2.9)$$

$$F_r = -\mu\ddot{z} - \lambda\dot{z} \quad (2.10)$$

which uses the incident wave elevation, η , and its first two derivatives. Assuming the body is located at the origin, $x = 0$, the elevation, velocity, and acceleration of a water particle on the surface of a regular wave are described using linear wave theory as

$$\eta = \frac{H}{2} \cos(-\sigma t) \quad (2.11)$$

$$\dot{\eta} = \frac{H}{2}\sigma \frac{\sinh k(h+z)}{\sinh kh} \sin(-\sigma t) \quad (2.12)$$

$$\ddot{\eta} = -\frac{H}{2}\sigma^2 \frac{\sinh k(h+z)}{\sinh kh} \cos(-\sigma t) \quad (2.13)$$

and if an irregular wave is used, equations 2.11 through 2.13 are found for each component wave and summed to find the resultant irregular wave.

The added mass, μ , and radiation damping term, λ , were derived from [15] using an eight meter diameter cylinder with a draft of four meters. The added mass at infinite frequency was used, and the radiation damping term was approximated as a constant according to the energy wave period of the sea state tested. The buoyant force is calculated as

$$F_b = -Kz = -\rho g \pi r^2 z \quad (2.14)$$

where ρ is the density of sea water, g is the acceleration due to gravity, r is the float radius, and z is the buoy displacement from equilibrium.

Substituting Eqns. 2.10 and 2.14 into Eqn. 2.8, the state equation of the buoy is obtained,

$$\ddot{z} = \frac{1}{m + \mu}(-\lambda \dot{z} - Kz - F_{pto} + F_e). \quad (2.15)$$

The hydrodynamic model was then coupled to both the passive and active hydraulic PTO systems described in the next two sections.

2.4 Hydraulic Power Transmission Modeling

Two hydraulic power transmissions were modeled in this research. A passive hydraulic system uses a set of check valves to rectify the flow and accumulators to smooth the power output and provide energy storage. The active hydraulic system uses a variable displacement hydraulic motor/pump and active damping control to continuously change the system response to track an optimal velocity profile.

The hydraulic models were developed assuming turbulent flow and neglecting line losses and other geometrical dissipative effects. As a basis of comparison, both

the passive and active systems use the same size buoy, pump, and hydraulic motor.

2.4.1 Passive Hydraulic PTO

The passive hydraulic system shown in Figure 2.4 contains a double acting hy-

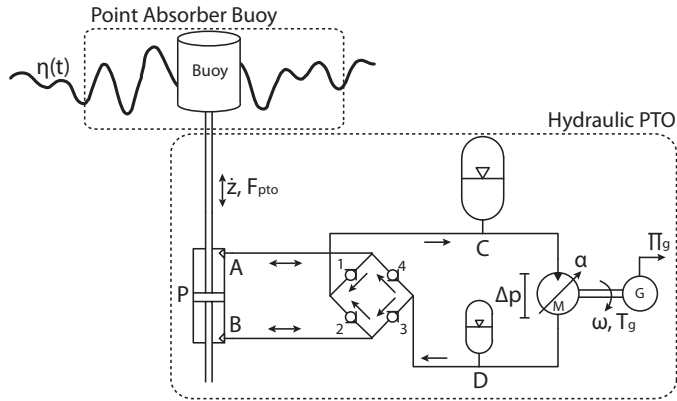


Figure 2.4: Schematic of the passive WEC system. The arrows indicate the direction of flow.

draulic piston pump, labelled “P”, to transform the linear kinetic energy of the heaving buoy into a pressurized fluid flow. The bidirectional flow from ports “A” and “B” of the pump is rectified by four one-way valves, labelled “1-4”, and delivered to the high pressure side. The high pressure accumulator, “C”, stores hydraulic energy and smooths the flow across the motor. A variable displacement motor, “M”, translates the hydraulic fluid power into rotational energy to spin a generator, “G”. The fluid then enters the low pressure side where accumulator “D” provides a pressurized reservoir for the hydraulic fluid. The pump draws fluid from the reservoir as needed to complete the circuit.

The hydraulic PTO model is described by Eqns. 2.16 through 2.24. The pressure in line “A” and “B” is expressed, using the continuity equation for a compressible fluid [11], as

$$\dot{p}_A = \frac{\beta_e}{V_0 - A_p z} (A_p \dot{z} - \dot{V}_1 + \dot{V}_4) \quad (2.16)$$

$$\dot{p}_B = \frac{\beta_e}{V_0 + A_p z} (-A_p \dot{z} - \dot{V}_2 + \dot{V}_3) \quad (2.17)$$

where β_e is the effective bulk modulus of the hydraulic fluid, V_0 is the initial volume of the cylinder, A_p is the piston area, and \dot{V}_1 through \dot{V}_4 are the volumetric flows through each check valve with a corresponding numeric label in Figure 2.4. The piston is assumed to be directly coupled to the buoy, therefore the velocity of the piston, \dot{z} , is the same as the buoy.

The flow across each valve in Eqn. 2.18 is modeled using the orifice equation,

$$\dot{V}_i = C_d A_v \sqrt{\frac{2}{\rho} (p_j - p_k) \tanh(k_1(p_j - p_k))}; \quad i = 1, 2, 3, 4 \quad (2.18)$$

where C_d is the discharge coefficient, A_v is the area of the orifice described by Eqn. 2.19, and p_j and p_k are the pressures on either side of the valve. The tanh function multiplied by the pressure difference provides an analytic approximation to the absolute value function, where $k_1 \gg 0$. The valve area is modeled as a variable area poppet valve,

$$A_v = \frac{A_{max} - A_{min}}{2} + A_{min} + \frac{A_{max} - A_{min}}{2} \tanh(k_2(p_j - p_k) - \frac{p_{max} + p_{min}}{2}) \quad (2.19)$$

where A_{max} and A_{min} are the maximum and minimum valve areas, p_{min} is the cracking pressure, and p_{max} is the pressure for which the valve is fully opened. The tanh function provides a smooth approximation to the piecewise operation of the valve, where k_2 is chosen such that when Δp is equal to the cracking pressure the valve area is equal to A_{min} . The behavior of the valve can be seen in Figure 2.5.

The flow into accumulator “C” and “D” is described by

$$\dot{V}_C = -\alpha D \omega + \dot{V}_1 + \dot{V}_2 \quad (2.20)$$

$$\dot{V}_D = \alpha D \omega - \dot{V}_3 - \dot{V}_4 \quad (2.21)$$

where the flow across the motor is found using the swashplate angle ratio, α , the

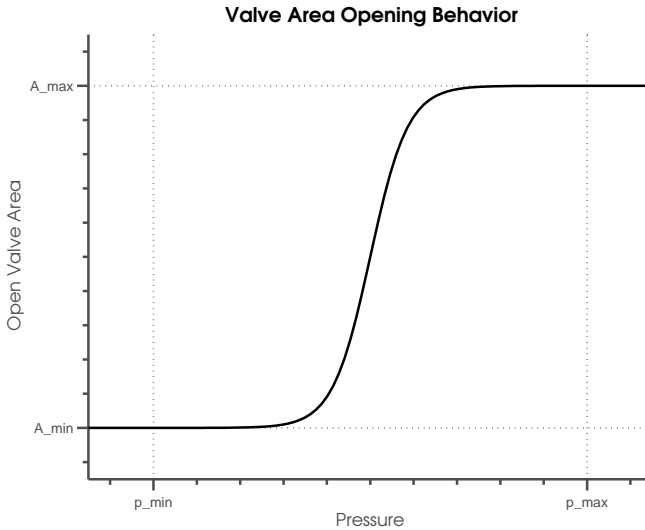


Figure 2.5: Valve opening behaviour as a function of pressure difference across the valve.

nominal motor displacement, D , and the rotational speed of the generator, ω . The swashplate angle ratio is a control input to vary the volumetric flow across the motor. The ratio represents the instantaneous motor displacement to the maximum motor displacement. For the passive system the swashplate angle ratio is fixed for the simulated sea state.

The pressure in each accumulator is dependent on the instantaneous volume of oil in the accumulator, related by

$$p_i = \frac{p_{i0}}{(1 - V_i/V_{i0})^{1.4}}; \quad i = C, D \quad (2.22)$$

where p_{i0} is the precharge pressure and V_{i0} is the total volume of the accumulator.

A torque balance on the hydraulic motor and generator drive leads to the state equation

$$\dot{\omega} = \frac{1}{J_t} (\alpha D(p_C - p_D) - b_g\omega - b_f\omega) \quad (2.23)$$

where $b_g\omega$ is the generator torque, $b_f\omega$ is the frictional torque, and J_t is the total

mass moment of inertia of the motor/generator drive train. The frictional damping used was one that would give the generator a 95% efficiency at a speed of 2400 rpm.

The PTO force in Eqn. 2.15 is determined by the pressure difference between sides A and B of the pump and the pressurized area of the piston, A_p .

$$F_{pto} = (p_A - p_B)A_p \quad (2.24)$$

2.4.2 Active Hydraulic PTO

The active system, shown in Figure 2.6, consists of a double acting piston cylinder

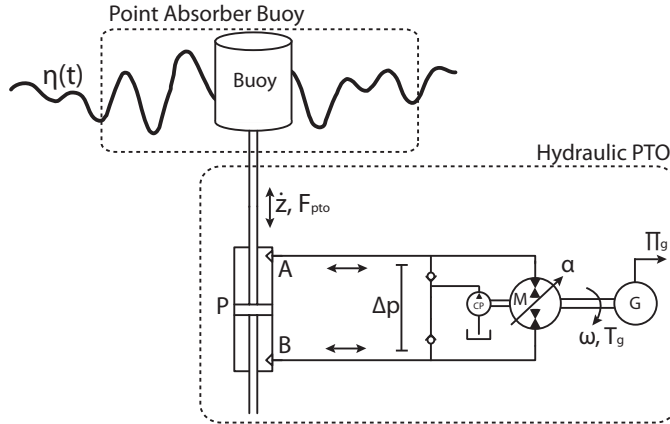


Figure 2.6: Schematic of the active WEC system.

directly connected to a variable displacement motor/pump. The swashplate angle ratio, “ α ”, can move from positive to negative displacement allowing rectification of the rotational motion of the pump/motor. A charge pump, “CP”, provides replenishing flow to the lines. The model is described by Eqns. 2.25 and 2.26. The PTO force is again given by Eqn. 2.24.

The pressure across the cylinder is found using the continuity equation for a

compressible fluid,

$$\Delta \dot{p} = \frac{\beta_e}{V_0 - A_p z} (-\alpha D \omega - C_t \Delta p + C_i p_{cp} + A_p \dot{z}) \quad (2.25)$$

where β_e is the effective bulk modulus of the fluid, A_p is the area of the piston, α is the swashplate angle ratio, D is the maximum displacement of the motor, C_t is the total leakage coefficient, and C_i is the total internal leakage coefficient [11]. The piston is assumed to be directly coupled to the wave buoy, therefore the displacement and velocity of the piston, z and \dot{z} are the same as the buoy. One of the lines is assumed to be at the charge pump pressure while the other line is pressurized; therefore only a single equation is needed to define the pressure in the pump.

A torque balance of the hydraulic motor and generator gives,

$$\dot{\omega} = \frac{1}{J_t} (\alpha D(p_A - p_B) - b_g \omega - b_f \omega - 0.1 D p_{cp}) \quad (2.26)$$

where J_t is the total moment of inertia of the coupled motor/generator, b_g is the generator damping, ω is the rotational velocity, and b_f is the frictional damping. The last term represents the torque required to run the charge pump specified as 10% of installed displacement and operating at a constant pressure, p_{cp} , of 2 MPa [30].

2.4.2.1 Linear Quadratic Tracking Controller for the Active Hydraulic PTO.

To maximize the power absorption of the buoy, an optimal velocity reference trajectory

$$\dot{z}_{opt} = \frac{F_e}{2\lambda} \quad (2.27)$$

is tracked [7, 1]. The reference trajectory is tracked using a Linear Quadratic Tracking (LQT) controller [24]. The controller seeks to minimize the quadratic

objective function,

$$J = \int_0^{t_f} [(\xi - \tilde{\xi})^T Q (\xi - \tilde{\xi}) + u^T R u] dt \quad (2.28)$$

where $\tilde{\xi}$ is the reference state to be tracked, u is the system input, and Q and R are weighting matrices used to tune the controller. The system state, ξ , is given by the dynamics

$$\dot{\xi} = A\xi + Bu, \quad (2.29)$$

where A is the system dynamics matrix and B is the input matrix.

Equations 2.15, 2.25, and 2.26 were first transformed into a system of first order differential equations,

$$\begin{aligned} \dot{\xi} &= f(\xi, u) \\ \xi &= [z, \dot{z}, \Delta p, \omega]^T \\ u &= [\alpha, b_g]^T \end{aligned} \quad (2.30)$$

then linearized around an operating point, $[\xi_o, u_o]$. The linearized system is

$$\dot{\xi} = f(\xi_o, u_o) + A\hat{\xi} + B\hat{u} + DF_e(t). \quad (2.31)$$

where $f(\xi_o, u_o)$ is the original, first order, non-linear system of equations evaluated at the operating point, $\hat{\xi}$ and \hat{u} is the deviation state vector about the operating point,

$$\begin{aligned} \hat{\xi} &= \xi - \xi_o \\ \hat{u} &= u - u_o \end{aligned} \quad (2.32)$$

and $DF_e(t)$ is a vector of the external forcing which enters in through equation

2.15 as the excitation force. Matrices A and B given by

$$A = \left. \frac{\partial f(\xi, u)}{\partial \xi} \right|_{\xi_o, u_o} \quad B = \left. \frac{\partial f(\xi, u)}{\partial u} \right|_{\xi_o, u_o} \quad (2.33)$$

are the linearized system dynamics matrix and linearized system input matrix respectively.

The minimization of Eqn. 2.28 produces the control law for the LQT controller given as

$$u(t) = -K_{LQR}\xi(t) - R^{-1}Bb(t) \quad (2.34)$$

where K_{LQR} is the Linear Quadratic Regulator (LQR) gain matrix obtained by solving the LQR problem about the operating point, and $R^{-1}Bb(t)$ is the feed forward input which accounts for the changing reference trajectory.

To find the LQR gain matrix in the first term of Eqn. 2.34, the built-in Matlab LQR function was used by specifying the Q and R matrices along with the linearized system dynamics matrix, A , and the linearized input matrix, B . The weighting matrices Q and R were chosen such that the actuation limits of the generator and swashplate were respected and the input and output power of the active system matched that of the passive system in the regular wave sea state.

The second term in Eqn. 2.34 is found by solving the differential equation

$$\dot{b} = -(A - BK_{LQR})^T b - \Pi_{LQR}(A\tilde{\xi} - \dot{\tilde{\xi}}) \quad (2.35)$$

where Π_{LQR} is the solution to the Continuous Algebraic Riccati Equation returned by the Matlab LQR function. Equation 2.35 is integrated from the final time, t_f , to the initial time, thereby requiring forward knowledge of the reference signal of Eqn. 2.27 (i.e. excitation force). In this research, forward knowledge of the excitation force is assumed to be available. In an actual system the excitation force could be predicted from time series forecasting tools such as an autoregressive model [1], neural network, or Kalman filter using current and previous state information from the buoy or an observation buoy located nearby.

The final closed loop system can be written as

$$\begin{aligned}\dot{\xi} = & f(\xi_o, u_o) + (A - BK_{LQR})\hat{\xi} + BK_{LQR}\tilde{\xi} \\ & - BR^{-1}B^T b + \tilde{N}(\xi_o, u_o, \xi, u) + DF_e(t)\end{aligned}\tag{2.36}$$

where $\tilde{N}(\xi_o, u_o, \xi, u)$ are the higher order terms of the Taylor series expansion that were neglected in the linear controller design.

Chapter 3: Simulation Results

3.1 Time Domain Simulation

Two hydraulic systems were simulated in Matlab using a variable step ordinary differential equation (ODE) solver. Each system was simulated using identical regular and irregular wave time series. Regular waves with a height of three meters and period of ten seconds and irregular waves with a significant height of three meters and energy period of 10 seconds were used because this condition represents high extraction potential off the coast of Oregon [25]. The systems were also simulated in an irregular fully-developed sea state constructed using a modified Bretschneider-Mitsuyasu spectrum [39].

As a basis for comparison, each hydraulic PTO system was coupled to the same heaving body point absorber model. In addition, the same size pump and motor was used for each system. Both systems were initially tuned in monochromatic waves to have equivalent efficiencies defined as the ratio of average power output by the generator to the average power absorbed by the hydraulic piston given by

$$\bar{\Pi}_{gen} = \frac{1}{t_f - t_0} \int_{t_0}^{t_f} T_g \omega \, dt \quad \bar{\Pi}_{hyd} = \frac{1}{t_f - t_0} \int_{t_0}^{t_f} F_{pto} \dot{z} \, dt. \quad (3.1)$$

The steady state response for each system was used for the analysis of each system. First the system parametrization is given, then simulation output of the behaviour and performance of each system is shown.

3.2 System Parameters

The parameters used for each simulation are given in Tables 3.1 through 3.3. The initial conditions were chosen such that the systems are at equilibrium in the

absence of an excitation force. Parameters for the sizing of the hydraulic PTO components were found using the design equations in Appendix A.

The hydrodynamic parameters in Table 3.1 are representative of an eight meter diameter cylinder with a draft of four meters. Experimental data for the parameters was used from [15]. A polynomial curve was fit to the experimental data so that a function could call values for a given sea state.

Table 3.1: Simulation parameters used for the point absorber buoy model.

Symbol	Parameter	Value
μ	Added mass	$7.825 \cdot 10^4$ kg
m	Physical mass	$8.694 \cdot 10^4$ kg
λ	Radiation damping	$1.572 \cdot 10^5$ kg/s
K	Hydrostatic stiffness	$2.843 \cdot 10^5$ kg/s ²

The passive system parameters used are given in Table 3.2. The bulk modulus was found in [11] for a hydraulic fluid with a density of 850 kg/m³. The parameters for piston area, high pressure accumulator volume, swash plate angle ratio, and generator damping are varied in the next chapter. The parameters were chosen for the passive system to maximize the power output in regular waves while maintaining the same hydraulic motor and piston sizes as the active system.

The active system parameters are listed in Table 3.3. The leakage coefficients are such that at the maximum pressure of 40 MPa, the system has a volumetric efficiency of 90%, a reasonable value for hydraulic systems [12]. The charge pump pressure and displacement was found from data sheet recommendations for closed circuit hydraulic systems.

Table 3.2: Simulation parameters used for the passive hydraulic PTO system.

Symbol	Parameter	Value	Unit
A_p	Piston area	$2.35 \cdot 10^{-2}$	m^2
β_e	Effective bulk modulus	$1.86 \cdot 10^9$	Pa
V_0	Vol. Cylinder Chamber	$7.06 \cdot 10^{-2}$	m^3
V_{C0}	Vol. Accumulator C	7.50	m^3
V_{D0}	Vol. Accumulator D	3.00	m^3
p_{C0}	Precharge pressure C	13.2	MPa
p_{D0}	Precharge pressure D	6.60	MPa
C_d	Discharge coefficient	0.61	-
A_{max}	Maximum valve area	0.001	m^2
A_{min}	Minimum valve area	$1.00 \cdot 10^{-8}$	m^2
p_{max}	Maximum area pressure	0.100	MPa
p_{min}	Cracking pressure	0.075	MPa
ρ_o	Hydraulic fluid density	850	kg/m^3
D	Motor displacement	250	cm^3
α	Swashplate angle ratio	1.00	-
b_g	Generator damping	2.375	$\text{kg m}^2/\text{s}$

Table 3.3: Simulation parameters used for the active hydraulic PTO system.

Symbol	Parameter	Value	Unit
A_p	Piston area	$2.35 \cdot 10^{-2}$	m^2
β_e	Effective bulk modulus	$1.86 \cdot 10^9$	Pa
V_0	Vol. cylinder chamber	$7.06 \cdot 10^{-2}$	m^3
p_{cp}	Charge pump pressure	2.00	MPa
C_t	Total leakage coefficient	$7.846 \cdot 10^{-11}$	$\text{m}^3/\text{Pa-s}$
C_i	Internal leakage coefficient	$1.400 \cdot 10^{-11}$	$\text{m}^3/\text{Pa-s}$
ρ_o	Hydraulic fluid density	850	kg/m^3
D	Motor displacement	250	cm^3

3.3 System Response

Average power values for both systems in regular and irregular waves are shown in Table 3.4. The system kinematics and wave elevation for the passive and active systems are shown for regular and irregular waves in Figures 3.1a and 3.1b. The optimal velocity trajectory according to Eqn. 2.27 is also shown.

The excitation and PTO force are shown in Figures 3.2a and 3.2b for both systems in regular and irregular waves respectively. The active system has a smoother profile, though with larger and more variable forcing. The passive system shows higher frequency components, but lower amplitude forcing when the excitation force is small and the buoy is stalled. The smoothing effect of the accumulators in the passive system can be seen as the forcing profile plateaus and is limited at the peaks of the cycle.

The passive system shows the buoy motion can be stalled for part of the cycle until a large enough excitation force causes the buoy to move. When the excitation force is low, there is not enough pressure on the piston side to open the check-valves. Figure 3.4 shows the system pressure and forcing when this phenomenon occurs. Since the fluid is modelled as compressible and the valves have trapped the fluid on the piston side, a spring-like effect occurs where the pressure on the piston side oscillates and decays until there is enough excitation force to open the valves. The passive hydraulic system therefore manifests an intrinsic latching control [7].

Table 3.4: Average power input and output of each system.

	Active System	Passive System
Regular Waves		
$\bar{\Pi}_{gen}$	126 kW	126 kW
$\bar{\Pi}_{hyd}$	162 kW	162 kW
Irregular Waves		
$\bar{\Pi}_{gen}$	104 kW	84 kW
$\bar{\Pi}_{hyd}$	125 kW	104 kW

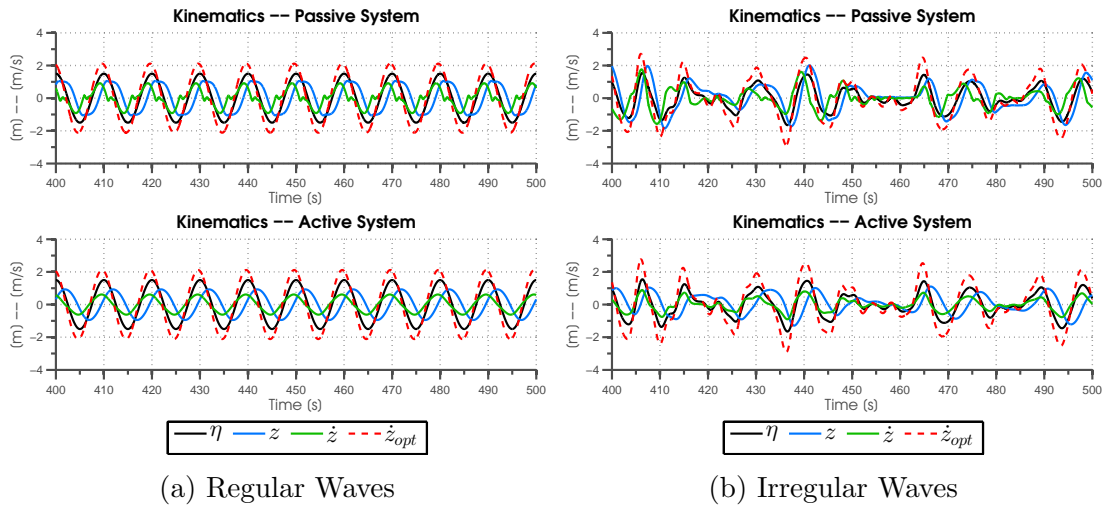


Figure 3.1: System kinematics and optimum velocity trajectory in regular and irregular waves.

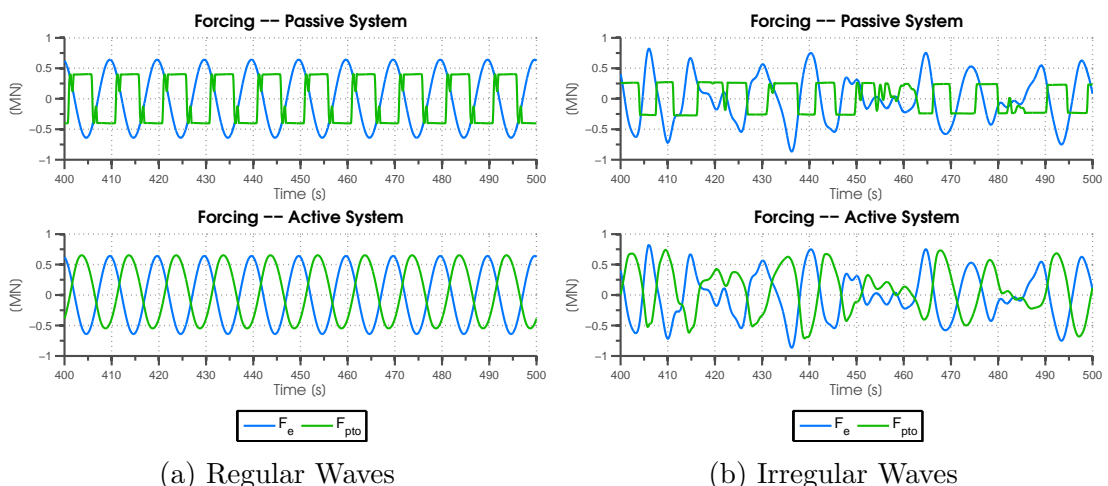


Figure 3.2: Excitation and piston forcing in regular and irregular waves.

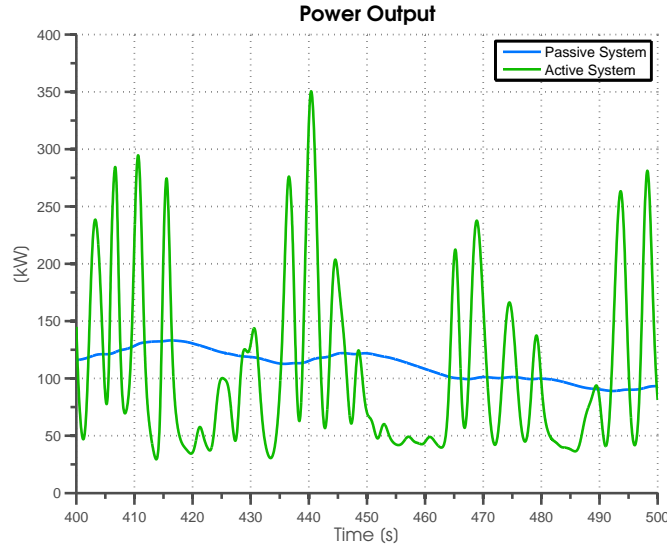
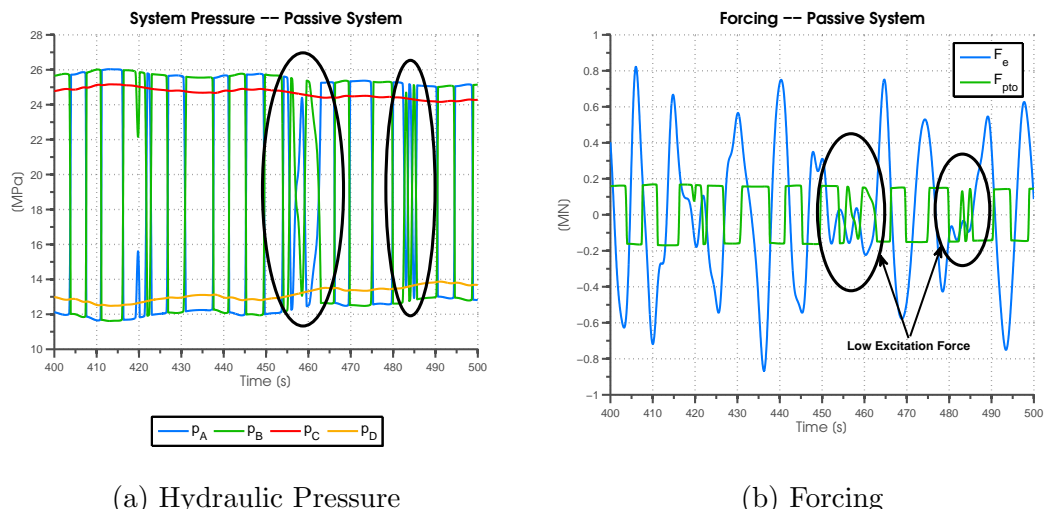


Figure 3.3: Power output for the passive and active hydraulic PTO systems.



(a) Hydraulic Pressure

(b) Forcing

Figure 3.4: System pressure and forcing when the stalling effect occurs in the passive system. A check valve is open when either pressure in sides A or B are greater than side C or less than side D.

Chapter 4: System Analysis

4.1 Loading Analysis of the Nominal Systems

Fatigue damage from the cyclic, irregular loading of ocean waves poses a significant design challenge for wave energy converters due to the stochastic nature of the loading. Understanding the expected loads a system will endure early in the design process will allow the development of more reliable and survivable WECs. To this end a loading analysis was conducted for the passive and active WEC systems in order to gain insight into the design requirements necessary to protect against fatigue damage.

The following presents a brief description of fatigue failure theory for fluctuating stresses. For a thorough explanation of the theory, however, see [29, 34]. Fatigue damage occurs when cyclic loading on a member perpetuates crack growth until the part eventually fractures and fails. A purely sinusoidal loading time series can be broken down into a mean, or steady component and an amplitude component as shown in Figure 4.1.

Each period of the fully reversed stress is counted as one cycle. When the time series is irregular, a rainflow counting algorithm is used to count and determine the amplitude and mean value of each stress cycle. The amplitude and mean value of each stress cycle is then used with a failure criterion such as the Modified Goodman method given by

$$S_f = \frac{\sigma_a}{1 - (\sigma_m/S_{ut})} \quad (4.1)$$

to determine the associated fatigue stress imparted by the cycle. A fatigue strength-life (S-N) curve, such as the one in Figure 4.2, relates the number of cycles to failure to a particular fatigue strength. A cumulative damage theory, such as the popular Palmgren-Miner rule, is then used in conjunction with the S-N curve to determine the contribution of each cycle fatigue strength value to the fatigue damage of the

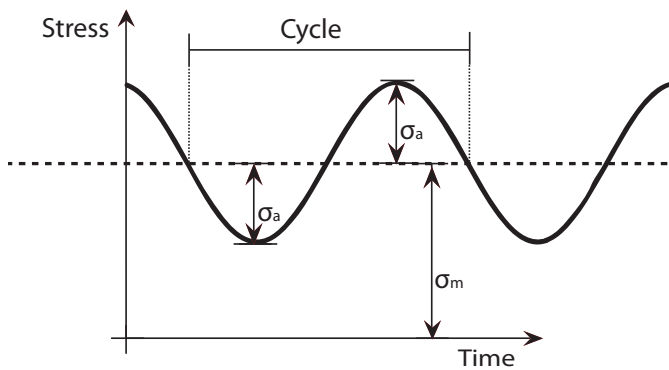


Figure 4.1: An example of a purely sinusoidal fully reversed stress time series. The amplitude, σ_a , and the mean value, σ_m , characterize the stress history.

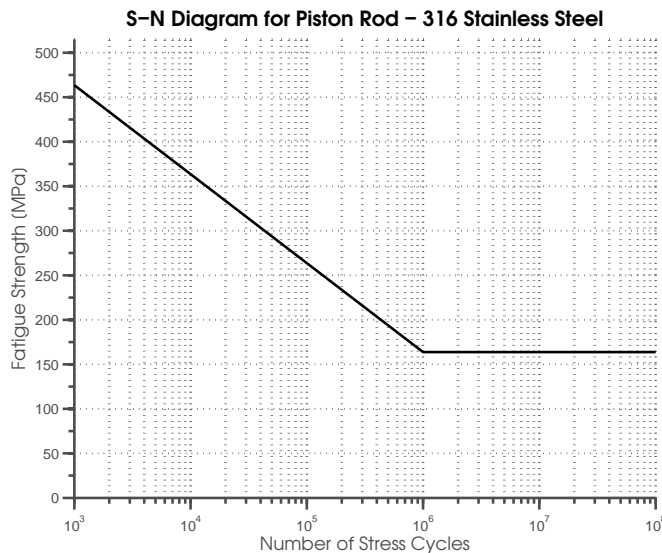


Figure 4.2: An example S-N curve for 316 stainless steel. The knee of the curve is called the endurance limit. Any calculated fatigue strength cycles below this point will not contribute to fatigue damage. The sloped region of the curve constitutes the finite-life regime where cycles will contribute to damage.

component. If the cumulative fatigue damage from all previous cycles reaches the total allowable damage, then the part is said to have failed.

The understanding of loading cycles can be used to design structures and components that will withstand the expected cyclic loading. For steel beam design, this amounts to specifying the cross-sectional area of the beam to be large enough to limit the majority of forcing to below the endurance limit, thereby ensuring long life. For bearings and nonferrous materials, no endurance limit exists and therefore knowledge and prevention of high magnitude loadings will prolong the component life.

The analysis that follows presents a characterization of the forcing time histories experienced by the piston and generator shafts for a common energetic sea state. The piston and generator forcing were analyzed because they are major components that will experience the brunt of the loading from ocean waves. The loading time series are also directly obtainable from the dynamic simulations described in the previous chapters. By understanding the forcing, the analysis can remain generic and avoid specifying any component sizes or materials — a job best left to the designer. The intent of the loading analysis is to allow developers and designers to gain an insight into the distribution of loading a particular device might experience.

A time series profile of the hydraulic piston force and motor torque profiles can be seen in Figure 4.3. It is observed that the active system has higher peak forcing on both components compared to the smoother profile of the passive system. The accumulators of the passive system provide pulsation damping and energy storage, and therefore the force on the piston is limited and the generator torque has a smoothed profile. The active system uses the generator torque along with the swashplate angle to provide force control of the piston in order to track the optimum velocity. The torque for the active system is therefore much more variable with higher peak amplitudes.

The systems were simulated in 30 minutes of irregular waves with a significant wave height of three meters and an energy period of ten seconds. A rainflow count-

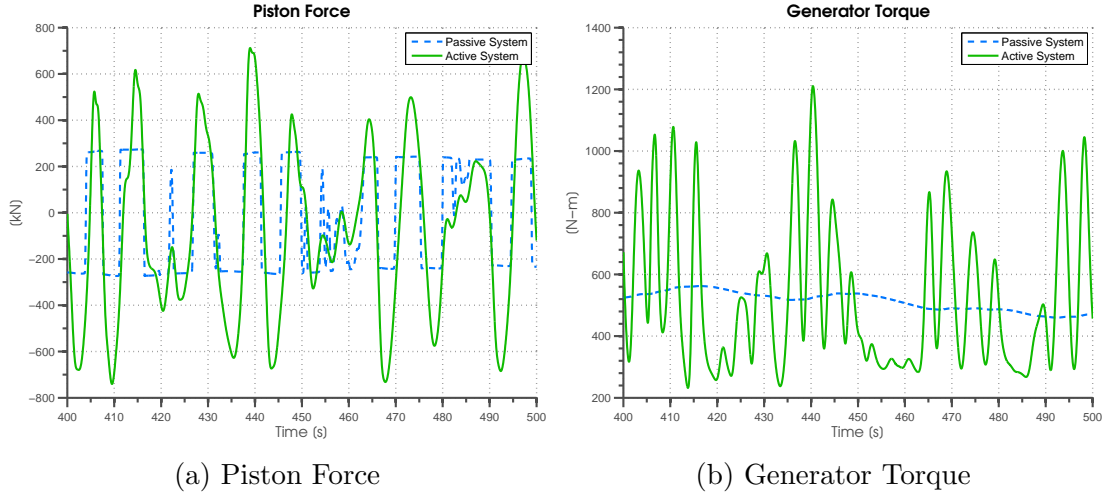


Figure 4.3: Time series of the loading for the two systems in irregular waves with a significant height of 3 meters and an energy period of 10 seconds.

ing algorithm was then used to count the number of irregular forcing cycles [22, 29]. The counted cycles were then binned and divided by the total number of cycles for each system to obtain a load probability, $P(x)$, where x is an individual load bin. Histograms of the full range amplitude and mean loading components for the piston rod and generator shaft were then created, shown in Figure 4.4.

Statistics for the distributions shown in Figure 4.4 are given in Table 4.1. The average load cycle was calculated from the distributions by,

$$\mu_{cyc} = \frac{x \cdot P(x)}{n} \quad (4.2)$$

where the product of each load bin, x , and corresponding load probability, $P(x)$ is summed over the total number of bins, n .

The piston and generator amplitude loading show the active system to have a wider distribution, which is confirmed by referring back to Figure 4.3. The passive system has many more low amplitude cycles due in part from the spring effect when the fluid is trapped on the piston side during periods of low excitation force. The piston mean loading is centered about zero for both systems, however the

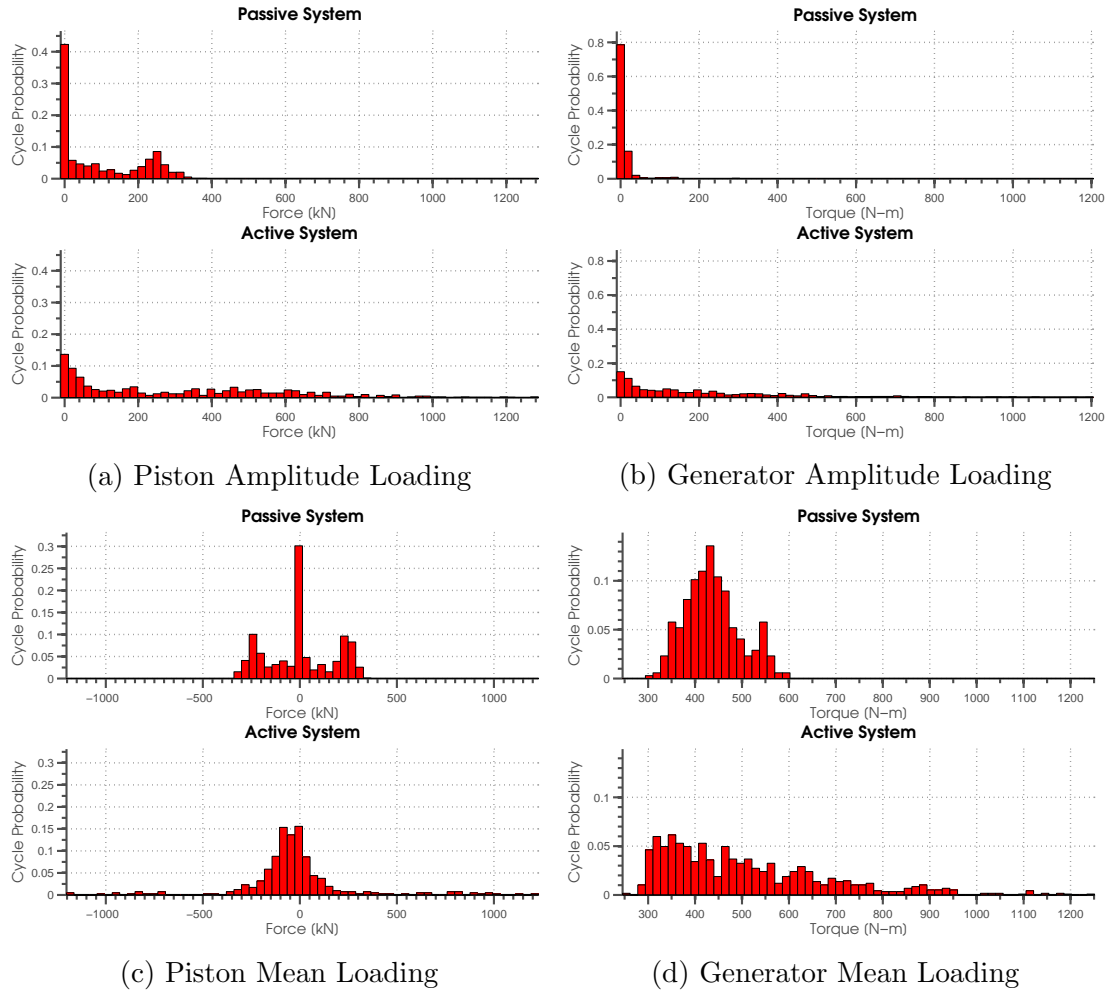


Figure 4.4: Piston and generator mean and amplitude loading distributions for a 30 minute irregular sea state.

Table 4.1: Piston and generator loading statistics for each system.

	Piston		Generator	
	Passive	Active	Passive	Active
Amplitude				
Total # Cycles	976	411	173	585
Average [kN]	96	307	8	195
Max [kN]	371	1277	301	1195
Mean				
Total # Cycles	976	411	173	585
Average [kN]	2	-32	437	505
Max [kN]	335	1210	592	1243
Min [kN]	-332	-1183	301	254

passive system has two additional means centered around $\pm 250\text{ kN}$. These low amplitude cycles are superimposed on the plateaus of the square wave and are the result of fluid entering and leaving through the check valves. The accumulators provide a nearly constant pressure when the check valves are open. However, since the gas dynamics are modeled, the additional input of fluid to the high pressure side increases this force slightly. The cycle amplitude therefore is low, but the mean is high during the plateau of the force. The generator means have similar values, though the active system has a wider distribution with a slowly tapering tail.

The distribution of loading cycles with respect to both the mean and amplitude components is shown in Figures 4.5 and 4.6. These histograms show a more complete picture of the loading and illuminate some rather interesting characteristics of the two systems.

The passive system piston and generator histograms are shown in Figure 4.5. The tri-modal mean distribution for the piston confirms the low amplitude contribution from the mirrored means. The high amplitude, zero mean peak is the result of a change in direction of the buoy from the alternating excitation force. The low cycle probabilities forming a triangle-like distribution between the peaks is partly due to the spring-like effect of trapped fluid on the piston side during periods of

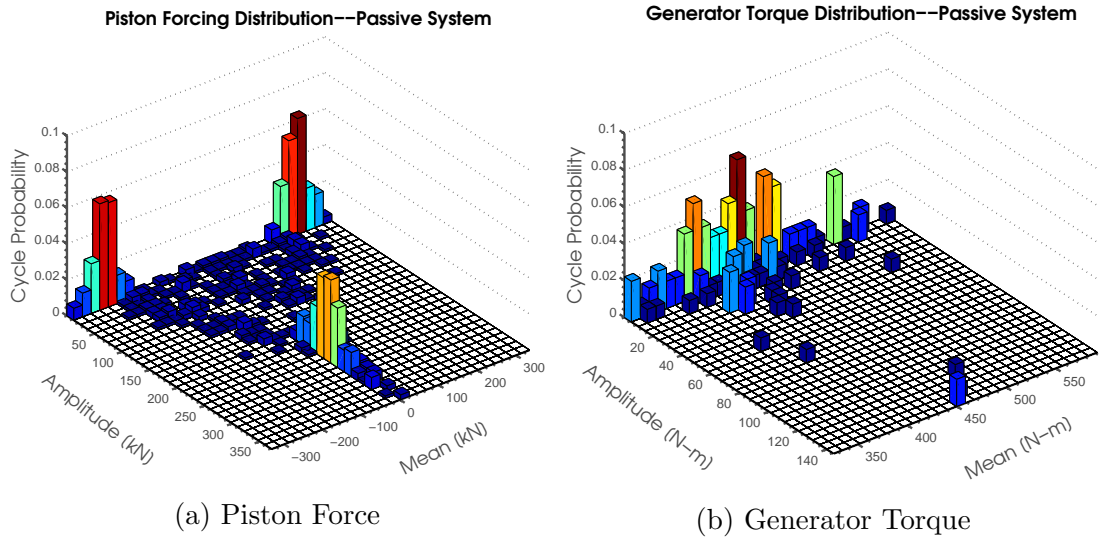


Figure 4.5: Loading distribution of the passive system with respect to mean and amplitude values for irregular waves with a significant height of 3 meters and an energy period of 10 seconds.

low excitation force.

The generator distribution for the passive system shows a wide spread of low amplitude loading distributed between approximately 300 to 600 N-m. Referring back to Figure 4.3 it is noted that this low amplitude loading is due to the smoothing effect of the accumulators. The higher amplitude loadings occur less frequently over longer periods, a response more closely tied to the passing of wave groups rather than individual waves.

The histograms for the active system are shown in Figure 4.6. The active system piston loading distribution indicates a mostly zero mean spread with amplitudes relatively evenly distributed. The generator distribution shows the majority of loading occurs around 150 – 400 N-m and diminishes with increasing mean in a linear fashion. The active system has higher peak torques on the generator shaft because the controller sometimes commands large torques in order to track the optimal velocity trajectory.

The probability a cycle will occur over a certain threshold can be described

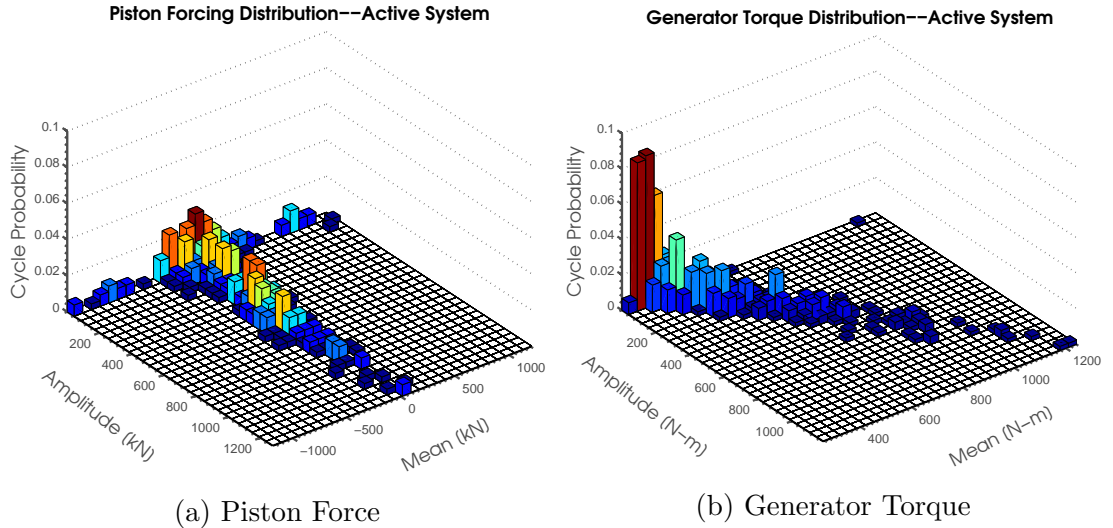


Figure 4.6: Loading distribution of the active system with respect to mean and amplitude values for irregular waves with a significant height of 3 meters and an energy period of 10 seconds.

by developing an exceedance histogram [13]. First the cumulative distribution function (CDF),

$$F(x) = \sum_{i=1}^n P(x = x_i) \quad (4.3)$$

was found by cumulatively summing the probabilities from the first to last bin. The CDF expresses the probability an event will occur that is less than a certain value. To obtain the probability a cycle will occur over a certain loading, the exceedance function was found,

$$\bar{F}(x) = 1 - F(x). \quad (4.4)$$

Inspection of Figures 4.5 and 4.6 indicate the amplitude loading of the piston and the mean loading of the generator will be of primary concern. The exceedance of these two loading components is shown in Figure 4.7.

The distributions for the piston amplitude loading indicate the active system

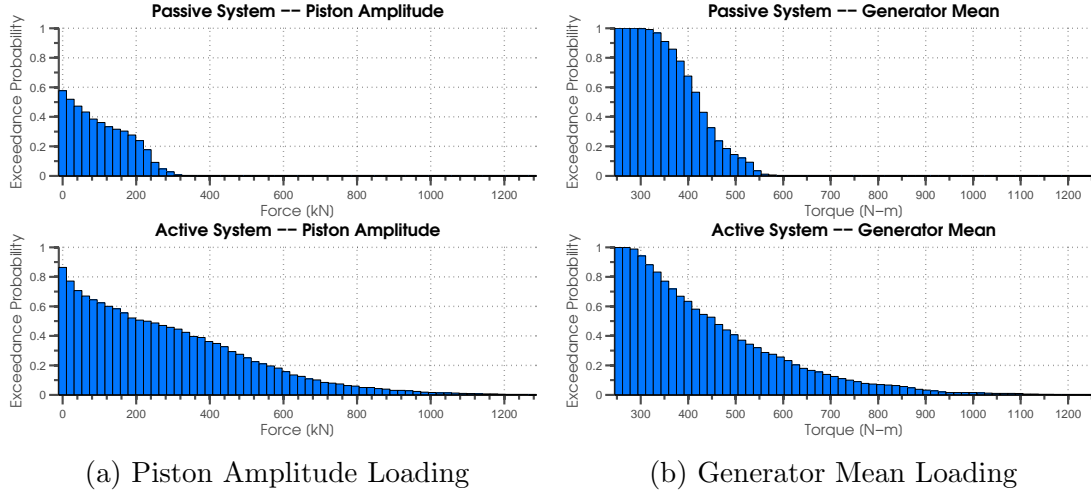


Figure 4.7: The exceedance probability of the rainflow counted loading cycles for irregular waves with a significant height of 3 meters and an energy period of 10 seconds.

to have much higher forcing for nearly any given exceedance probability. Roughly 10% of the time the amplitude loading was greater than 250 kN for the passive system, while the active system forcing exceeded this value nearly 50% of the time. This indicates a larger, more robust piston may be needed for the active system in comparison with the passive system. The generator mean loading indicates a similar situation where the active system is more likely to experience higher loading.

4.2 Variation of System Parameters for the Passive System

Parameters of the passive system were varied in order to understand how the loading and forcing is affected. With this understanding the designer can better weigh the cost and benefit of a particular device configuration. In all the analyses that follow, only a single parameter was changed while all other parameters remained as described in the previous chapter. Inspection of the passive system loading distributions indicate the piston amplitude and generator mean are of primary concern.

Therefore, histograms of the piston amplitude and generator mean are shown as the system parameters are varied.

The generator damping, hydraulic motor size, accumulator volume, and pump size were all varied because they represent the components a designer might manipulate in order to change the loading and power characteristics of the passive hydraulic system.

4.2.1 Variation of Generator Damping

The generator damping controls the amplitude of oscillation and power absorbed by the generator. Because the generator offers more resistance with higher damping values, higher fluid pressures over the motor will develop. Since the check valves open only when the fluid pressure on the piston is higher than the motor side, the piston force will necessarily increase with higher damping.

The generator damping was varied about the nominal value of approximately 2.5 kg/s, and histograms of the loading distributions are shown in Figure 4.8. The piston amplitude histogram shows a widening distribution as the damping is increased, while the mean distribution of the generator shifts upward in a linear manner.

The average power output according to equation 3.1 and the average loading for the piston and generator are shown in Figure 4.9. The average power reaches a maximum around the nominal damping value, indicating a well chosen damping value for the nominal system. Increasing the damping ratio will only lead to higher system forcing with no gain in power. A benefit could be had by reducing the generator damping slightly in order to lower the nominal loading if power absorption could be sacrificed.

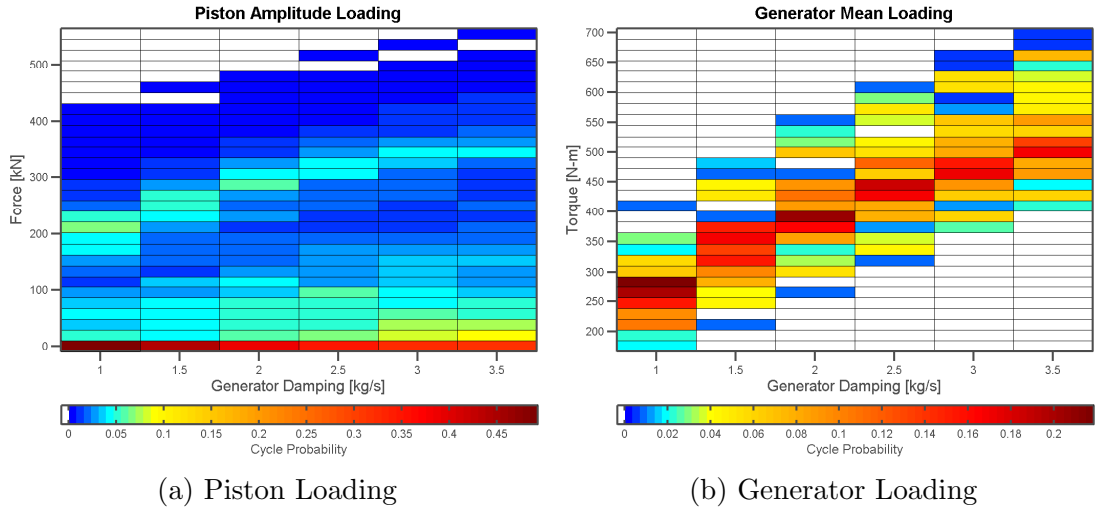


Figure 4.8: Loading distribution as the generator damping is changed. All other parameters are the same as listed in Tables 3.1 through 3.3.

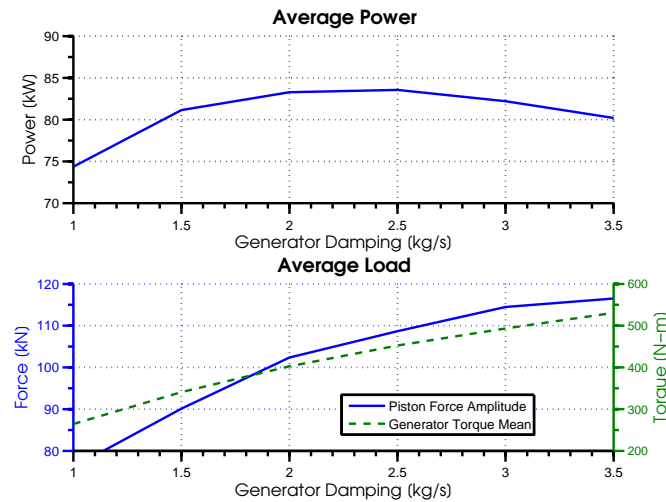


Figure 4.9: Average power and loading values as the generator damping is varied.

4.2.2 Variation of Motor Displacement

An increased motor displacement will allow a higher flow rate over the hydraulic motor and therefore the average volume and pressure of the accumulator will be lower. With a lower accumulator pressure, less force on the piston is necessary to open the check valves. By inspection of equation 2.23 and all else being equal, an increased motor displacement has the effect of lowering the mass and damping terms, thereby decreasing the phase and increasing the amplitude response of the motor.

The loading distributions indicate the piston amplitude loading converges with increasing motor displacement fraction while the generator mean loading widens as the fraction increases. The average of the piston amplitude loading decreases while the average generator mean loading remains relatively constant as shown in Figure 4.10.

The average generator power and average loadings are shown in Figure 4.11, where a peak power is noted at the nominal motor displacement. A decrease in piston amplitude forcing could be achieved by increasing the motor displacement, though the average power would decrease.

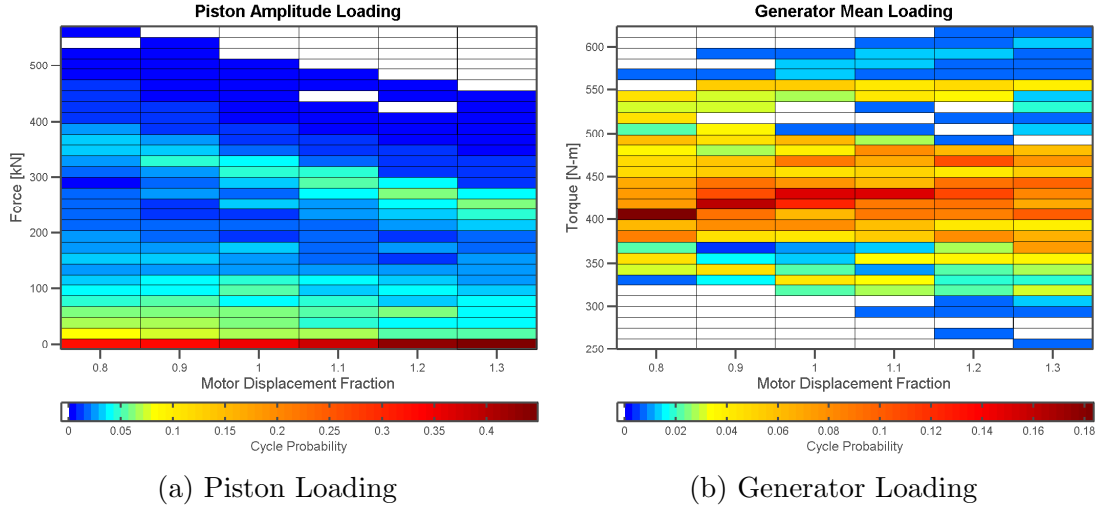


Figure 4.10: Loading distribution as the motor displacement ratio is changed. At $\alpha = 1$ the motor displacement is 250cm^3 . All other parameters are the same as listed in Tables 3.1 through 3.3.

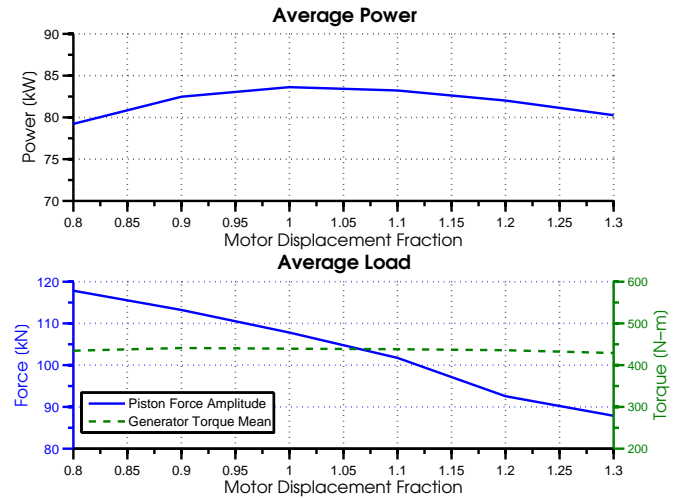


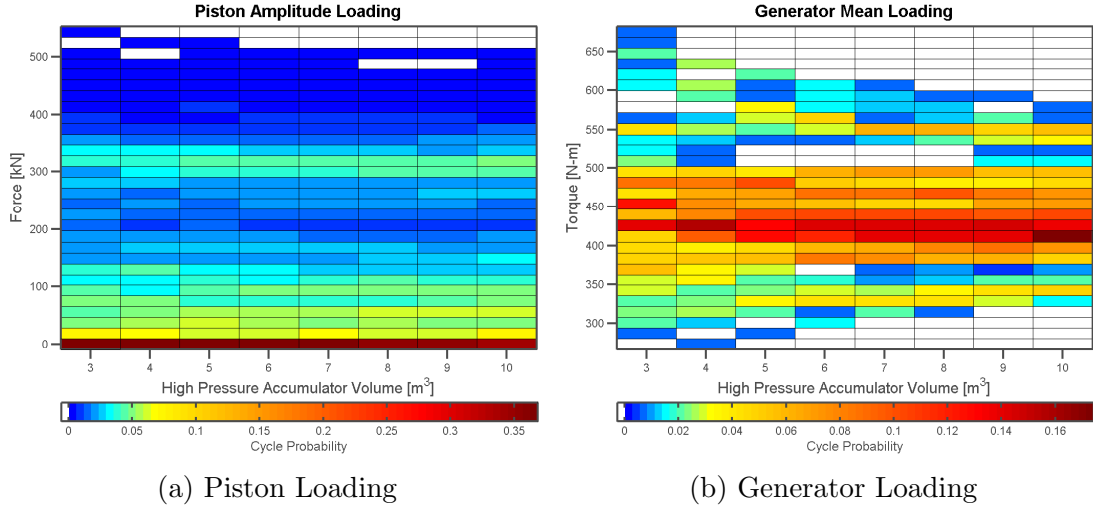
Figure 4.11: Average power and loading values as the motor displacement ratio is varied.

4.2.3 Variation of High Pressure Accumulator Volume

The high pressure accumulator volume was varied about the nominal accumulator volume of $7.5m^3$. Increasing the accumulator volume is analogous to increasing the capacitance, or energy storage capability of a system. With more energy being stored at any given instant, less energy is available at the output and therefore the overall input to output efficiency is lower. However, the increased energy storage capacity of larger accumulators can help to reduce variability and smooth the output power.

The loading distribution for the piston amplitude loading, shown in Figure 4.12, remains relatively constant throughout the range of values. As the accumulator volume increases, the pressure across the motor becomes more consistent and therefore the generator distribution converges.

Figure 4.13 shows the average power output decreases slightly as the accumulator volume is increased because more energy is being stored within the system. The average loading of both the piston and generator remains relatively consistent throughout the range.



(a) Piston Loading

(b) Generator Loading

Figure 4.12: Loading distribution as the high pressure accumulator volume is changed. At $v_{C0} = 7.5\text{m}^3$ the original system is shown. All other parameters are the same as listed in Tables 3.1 through 3.3.

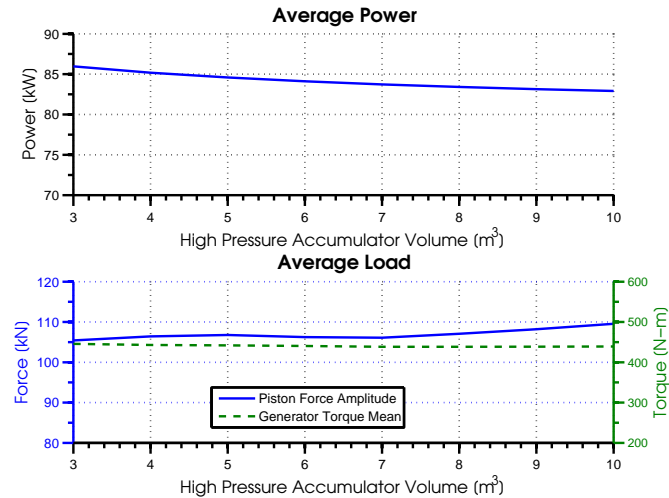


Figure 4.13: Average power and loading values as the high pressure accumulator volume is varied.

4.2.4 Variation of Pump Area

The pump size was varied by changing the pressurized area of the pump. The change in pump area is presented as a fraction of the nominal pump area. As the pump area is increased and the accumulator pressure remains relatively constant, a higher amplitude force will be produced on the piston.

The loading amplitude distributions are shown in Figure 4.14 where it is noted that the piston amplitude loading widens with increasing pump area. The generator loading widens slightly, but remains relatively consistent with increasing area.

The average power and loading are shown in Figure 4.15, where the power reaches a peak at the nominal pump area. The average amplitude for the piston increases with increasing pump area, and the generator mean remains consistent. Reduced forcing on the pump could be obtained by decreasing the pump area fraction, at the cost of reduced power.

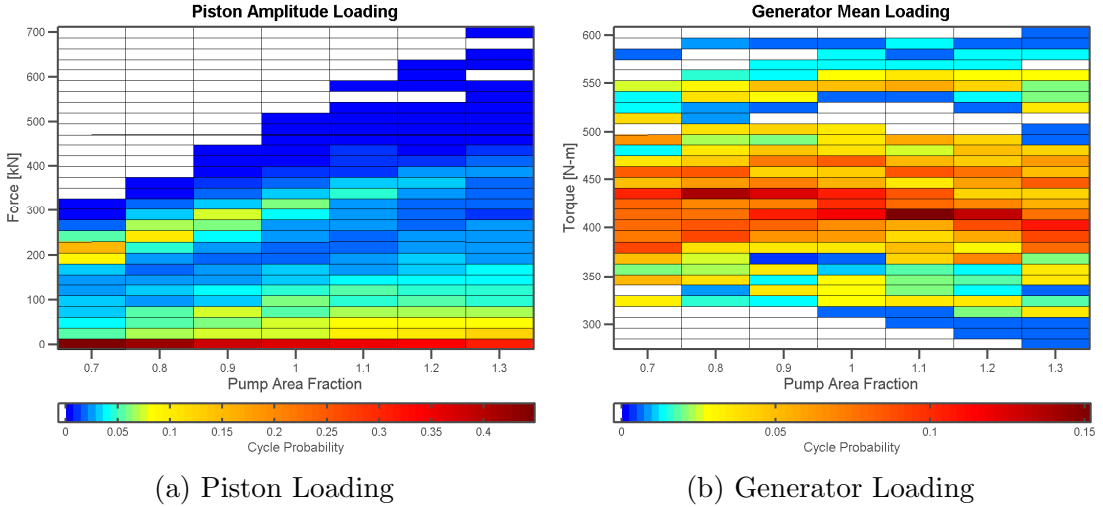


Figure 4.14: Loading distribution as the pressurized pump area fraction is changed. The pump area fraction is with respect to the original pump size. At $A_p = 1$ the original system is shown. All other parameters are the same as listed in Tables 3.1 through 3.3.

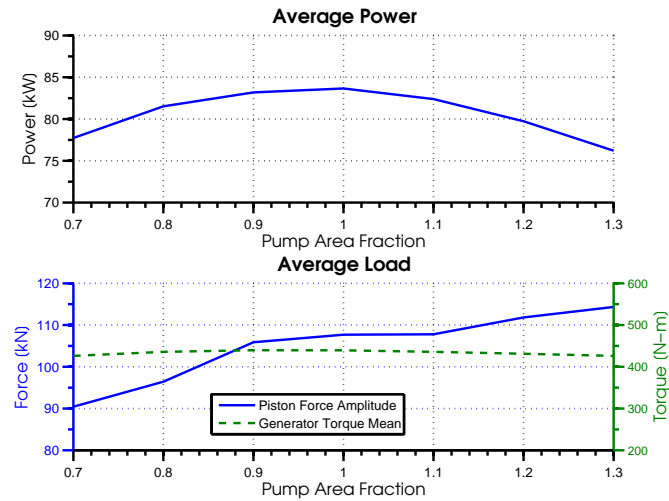


Figure 4.15: Average power and loading values as the generator pump area fraction is varied.

Chapter 5: Conclusions and Future Work

The potential for clean, renewable energy from ocean waves is possible and will undoubtedly contribute to the world's energy portfolio in the future. While great potential exists, much is still yet to be done and will take dedicated scientists, engineers, and developers to address key technological challenges.

Key challenges include improving the reliability and survivability of technologies and increasing conversion efficiencies in order to bring the cost of electricity to a competitive level. Reliability and survivability is directly related to the nature of loading; therefore in order to make improvements in this area design decisions must be made with understanding of the potential loads.

The work presented in this thesis attempts to shed light on the nature of loading between two popular hydraulic power take off configurations, a passive system tuned to the dominant forcing period of the sea state and an active system following an optimal power absorption trajectory. The knowledge of the nature of loading will help developers make informed decisions early in the design process. There is no 'right' technology, but rather well informed design decisions in order to overcome the key challenges to wave energy conversion.

Two hydraulic PTO systems coupled to a hydrodynamic point absorber were modeled then simulated in regular and irregular waves. The two systems were tuned to have the same input to output power ratios in regular waves. The systems were then simulated in irregular waves and analyses of the loading distribution for the piston and the generator were conducted. The analysis of the piston loading shows the passive system to have a converged distribution, but higher frequency loading. The active system generally has a wider distribution of piston forcing with higher peak to average loading variability. The generator loading distribution shows much higher variability in the actively controlled system as expected because the torque is manipulated to provide tracking control. The active system has higher

amplitude components and a wider range of mean components.

This work examined a passive system with accumulators to smooth the flow and an actively controlled system, with no direct hydraulic accumulation. A hybridized version of the two systems may lead to greater overall gains, with reduced loading variability and greater power absorption.

The hydrodynamic buoy was modelled as a single degree of freedom cylinder operating in heave with a constant radiative damping term to ease the control formulation. Hydraulic PTO systems are not limited to a heaving point absorber system, but could be used with WECs that take advantage of other modes of motion. Application of the hydraulic PTO models to different hydrodynamic models would be an interesting extension.

The two hydraulic models avoided specifying component efficiency functions, although this will be an important factor in the sizing and cost of components. Hydraulic efficiencies are a function of the pressure, flow rate, and viscosity of the working fluid. Incorporating hydromechanical and volumetric efficiency functions would lead to more realistic models.

A pressure relief valve to protect the systems against over-pressurization was not included in this work because the systems were designed to not over-pressurize in the sea state tested. Including pressure relief valves is necessary for an actual physical implementation of the system to avoid system damage in high sea states. Loads can be limited by setting the pressure relief valve to a nominal value. Understanding the loading distributions with this added component would be an important extension of this work.

A linear quadratic tracking controller was developed to control the active system. Other control techniques such as model predictive control, or learning based methods that can take into account actuator limits directly could give better overall performance. Furthermore, life extending controls suggested in [16, 36] offer a possible solution to reducing loading while maintaining high dynamic performance of an actively controlled WEC.

The actuation dynamics of the active system were not modeled for this research,

and therefore it is difficult to discern the energy storage requirements for the active system control. Incorporating actuation dynamics would give a better indication of the overall system requirements for both systems.

The electrical generator in this work was modeled as a simple linear damper. Furthermore, a power electronics system was assumed to exist to change the damping of the active system. Modeling an actual electrical machine and power electronics unit would produce a more realistic model and would be a beneficial future extension to the work.

Only a 30 minute simulation at one sea state was used for the loading analyses in this work. It would be an important extension to test a range of sea states where the device might be implemented. Because there is seasonal variation of the sea state at any location, further work could involve using a site resource assessment to base the frequency of simulations at particular sea states for a year of operation. Then, trends could be examined in the forcing distributions over an entire year of operation at a particular site.

Finally, as with any simulated system, the next logical step is to validate the models against physical implementations. System parameters such as losses and generator damping could then be assessed to improve the modeling.

The future of wave energy is promising and the work to date has merely scratched the surface. In order to progress the technologies, special attention must be paid to reliability, survivability, and increased power output in a range of sea states. This work has attempted to add to the body of knowledge and move the technologies toward realization.

Bibliography

- [1] T. K. A. Brekken. On model predictive control for a point absorber wave energy converter. In *PowerTech, 2011 IEEE Trondheim*, pages 1 – 8, 2011.
- [2] Ronan Costello, John Ringwood, and Jochem Weber. Comparison of two alternative hydraulic PTO concepts for wave energy conversion. In *Proceedings of the 9th European Wave and Tidal Energy Conference (EWTEC)*, 2011.
- [3] Robert G. Dean and Robert A. Dalrymple. *Water Wave Mechanics for Engineers & Scientists (Advanced Series on Ocean Engineering-Vol2)*. World Scientific Pub Co Inc, January 1991.
- [4] B Drew, A R Plummer, and M N Sahinkaya. A review of wave energy converter technology. *Proceedings of the Institution of Mechanical Engineers, Part A: Journal of Power and Energy*, 223(8):887–902, December 2009.
- [5] H. Eidsmoen. Simulation of a slack-moored heaving-buoy wave-energy converter with phase control. *Division of Physics, Norwegian University of Science and Technology. Trondheim, Norway. May*, 6, 1996.
- [6] Antnio F. de O. Falco. Wave energy utilization: A review of the technologies. *Renewable and Sustainable Energy Reviews*, 14(3):899–918, April 2010.
- [7] Johannes Falnes. *Ocean Waves and Oscillating Systems*. Cambridge University Press, 2005.
- [8] H. Yavuz, T. J. Stallard, A. P. McCabe, and G. A. Aggidis. Time series analysis-based adaptive tuning techniques for a heaving wave energy converter in irregular seas. *Journal of Power and Energy*, 221:77–90, 2007.
- [9] J. Hals. *Modelling and phase control of wave-energy converters*. PhD thesis, Norwegian University of Science and Technology, 2010.
- [10] Ross Henderson. Design, simulation, and testing of a novel hydraulic power take-off system for the pelamis wave energy converter. *Renewable Energy*, 31(2):271–283, February 2006.

- [11] Herbert E. Merritt. *Hydraulic Control Systems*. John Wiley & Sons, Inc., 1967.
- [12] Houman Hatami. Hydraulic formulary, 2012.
- [13] Jason Scott Roth. Statistical modeling of rainflow histograms. Master's thesis, University of Illinois at Urbana-Champaign, 1998.
- [14] John Andrews and Nick Jolley. *Energy Science: Principles, Technologies, and Impacts*. Oxford University Press, USA, 2007.
- [15] John V. Wehausen. Motion of floating bodies. In *Annual Review of Fluid Mechanics*, volume 3, pages 237 – 267.
- [16] C.F. Lorenzo and W.C. Merrill. Life extending control-a concept paper. In *American Control Conference, 1991*, pages 1081– 1095, 1991.
- [17] Laurence D. Mann. Application of ocean observations & analysis: The CETO wave energy project. In *Operational Oceanography in the 21st Century*, pages 721–729. Springer, 2011.
- [18] Michael E. McCormick. *Ocean Wave Energy Conversion*. Dover Publications, September 2007.
- [19] Stephen A. Meicke. Hydroelastic modeling of a wave energy converter using the arbitrary lagrangian-eulerian finite element method in LS-DYNA. 2011.
- [20] Gunnar Mork, Stephen Barstow, Alina Kabuth, and M. Teresa Pontes. Assessing the global wave energy potential. In *Proc. of 29th International Conference on Ocean, Offshore and Arctic Engineering, ASME, paper*, volume 20473, 2010.
- [21] Markus Mueller and Robin Wallace. Enabling science and technology for marine renewable energy. *Energy Policy*, 36(12):4376–4382, December 2008.
- [22] Adam Nieslony. Rainflow Counting Algorithm - MATLAB realease 7.1.0. <http://www.mathworks.com/matlabcentral/fileexchange/3026-rainflow-counting-algorithm>, January 30, 2013.
- [23] Dara O'Sullivan, James Griffiths, Michael G. Egan, and Anthony W. Lewis. Development of an electrical power take off system for a sea-test scaled offshore wave energy device. *Renewable Energy*, 36(4):1236–1244, April 2011.

- [24] Peter Dorato, Chaouki Abdallah, and Vito Cerone. *Linear-Quadratic Control*. Prentice Hall, 1995.
- [25] Pukha Lenee-Bluhm. The wave energy resource of the US pacific northwest. Master's thesis, Oregon State University, May 2010.
- [26] K. Rhinefrank, J. Prudell, and A. Schacher. Development and characterization of a novel direct drive rotary wave energy point absorber MTS-IEEE oceans conference proceedings. In *OCEANS 2009, MTS/IEEE Biloxi-Marine Technology for Our Future: Global and Local Challenges*, page 15, 2009.
- [27] Ken Rhinefrank, Alphonse Schacher, Joseph Prudell, Ted K. A. Brekken, Chad Stillinger, John Z. Yen, Steven G. Ernst, Annette von Jouanne, Ean Amon, Robert Paasch, Adam Brown, and Alex Yokochi. Comparison of direct-drive power takeoff systems for ocean wave energy applications. *IEEE Journal of Oceanic Engineering*, 37(1):35–44, January 2012.
- [28] P. Ricci, J. Lopez, M. Santos, P. Ruiz-Minguela, J.L. Villate, F. Salcedo, and A.F.deO. Falcao. Control strategies for a wave energy converter connected to a hydraulic power take-off. *IET Renewable Power Generation*, 5(3):234, 2011.
- [29] Richard Budynas and Keith Nisbett. *Shigley's Mechanical Engineering Design*. McGraw-Hill, 8 edition.
- [30] Rico H. Hansen, Torben O. Andersen, and Henrik C. Pedersen. Model based design of efficient power take-off systems for wave energy converters. May 2011.
- [31] Robert Thresher. The united states marine hydrokinetic renewable energy technology roadmap, April 2010.
- [32] K. Ruehl. Time-domain modeling of heaving point absorber wave energy converters, including power take-off and mooring. 2011.
- [33] Kristof Schlemmer, F. Fuchsmaier, N. Bemer, Ronan Costello, and Carlos Villegas. Design and control of a hydraulic power take off in an axi-symmetric heaving point absorber. In *Proceedings of the Ninth European Wave and Tidal Energy Conference, Southampton*, 2011.
- [34] Secil Ariduru. *Fatigue Life Calculation by Rainflow Cycle Counting Method*. PhD thesis, Middle East Technical University, 2004.

- [35] T. Stallard, G. P. Harrison, P. Ricci, and J. L. Villate. Economic assessment of marine energy schemes.
- [36] C. J Stillinger, T. K.A Brekken, A. von Jouanne, R. Paasch, D. Naviaux, K. Rhinefrank, J. Prudell, A. Schacher, and E. Hammagren. WEC prototype advancement with consideration of a real-time damage accumulation algorithm. In *PowerTech, 2011 IEEE Trondheim*, page 18, 2011.
- [37] M.J. Tucker and E.G. Pitt. *Waves in Ocean Engineering*. Elsevier Science, 1 edition, November 2001.
- [38] Y. Kamizuru, L. Verdegem, P. Erhart, C. Langenstein, L. Andren, M. LenBen, and H. Murrenhoff. Efficient power take-offs for ocean energy conversion. Dublin, October 2012.
- [39] Yoshimi Goda. *Random Seas and Design of Maritime Structures*, volume 33 of *Advanced Series on Ocean Engineering*. World, 3 edition.

APPENDICES

Appendix A: Design Equations for the WEC Systems

The systems were designed for a nominal irregular sea state with a significant height of three meters and energy period of ten seconds. In this sea state, the hydraulic system components were sized to deliver a rated power of 150 kW at a rated rotational speed of 2400 RPM. With knowledge of the rated speed, ω_r , and power, Π_r , the rated torque can be derived as

$$\tau_r = \frac{\Pi_r}{\omega_r} \quad (\text{A.1})$$

Multiple hydraulic motor sizes were compared and a 250 cm³ axial piston pump was found to satisfy the torque and speed constraints. Using the assumed motor volume per revolution, D , and the rated speed, the rated volumetric flow rate can be found as

$$\dot{V}_r = D\omega_r \quad (\text{A.2})$$

The nominal damping coefficient can be found with knowledge of the rated torque as

$$b_g = \frac{\tau_r}{\omega_r} \quad (\text{A.3})$$

The mean absolute value of the vertical velocity component at the surface of an irregular wave was used to obtain an estimate of the required pump speed.

$$\dot{\bar{z}}_{est} = E[|\dot{\eta}|] \quad (\text{A.4})$$

The estimate can be used to find an appropriate starting point for the piston pump.

$$A_{p,est} = \frac{D\omega_r}{\dot{\bar{z}}_{est}} \quad (\text{A.5})$$

The system was then empirically found to have a maximum power at a pressurized area 1.5 times the estimate.

